Atmospheric Research 243 (2020) 105002

Contents lists available at ScienceDirect

Atmospheric Research

journal homepage: www.elsevier.com/locate/atmosres

Measurements of light-absorbing impurities in snow over four glaciers on the Tibetan Plateau

Hewen Niu[a,b,*], Shichang Kang[a,d,e], Yuhang Wang[b], Chandan Sarangi[c,f], Dipesh Rupakheti[a], Yun Qian[c]

[a] State Key Laboratory of Cryospheric Science, Northwest Institute of Eco-Environment and Resources, Chinese Academy of Sciences, Lanzhou 730000, China
[b] School of Earth and Atmospheric Sciences, Georgia Institute of Technology, Atlanta, GA 30332, USA
[c] Atmospheric Sciences and Global Change Division, Pacific Northwest National Laboratory (PNNL), Richland, WA 99352, USA
[d] CAS Center for Excellence in Tibetan Plateau Earth Sciences, Beijing 100101, China
[e] University of Chinese Academy of Sciences (UCAS), Beijing 10049, China
[f] Department of Civil Engineering, Indian Institute of Technology, Madras, Chennai, Tamil Nadu 600024, India

ARTICLE INFO

Keywords:
Snowpack
Black carbon
Dust
CALIPSO
Tibetan Plateau

ABSTRACT

Black carbon (BC), dust, and organic carbon (OC) aerosols, when deposited onto the surface of glaciers, can absorb light and decrease the snow albedo. These impurities in snow are referred to as ILAIs (i.e., insoluble light absorbing impurities). Atmospheric chemical models have been extensively used to simulate the transport and deposition of atmospheric aerosols in glacierized areas. However, systematic investigations of ILAIs in snowpack of glaciers on the Tibetan Plateau (TP) are rare. In this study, observations of ILAIs in snow and simulations of ILAIs of atmospheric aerosol at surface over four glaciers on the TP have been analyzed. Strong correlation between BC and dust was found in surface aged-snow, and their correlation significantly varied with snowpit depth. BC and OC concentrations in snowpit tended to decrease with depth. Significant differences of ILAI concentrations among depth intervals reflect their diverse hydrophilicities, physiochemical properties and post-depositional processes in snowpit, offering important observational constraints on the related processes. Monthly variation of atmospheric ILAIs at surface over glaciers is characterized by distinct spatial heterogeneity. The statistical results show higher ILAI concentrations in the summer of 2015 than 2014, which is in qualitative agreement with CALIPSO observations, likely reflecting the effects of inter-annual variation of summer monsoon on snow ILAI loadings. Optical attenuation (ATN) of BC is gradually decreased with depth of snowpit, whereas the trend of mass absorption cross-section (MAC) of BC throughout the profile of snowpit is opposite to that of ATN. The scanning electron microscopy (SEM) imaging demonstrates that calcium and silicon rich particles dominate over biological, quartz and flying ash particles in the cryoconite, providing additional constraints on the sources of dust-in-snow and can facilitate better understanding of the physicochemical properties and climatic effects of particles in the glacial cryoconite.

1. Introduction

Black carbon (BC) is a major component of tiny soot particles generated by the incomplete combustion of raw coal, diesel oil, gasoline and biomass fuel, which largely absorbs sunlight radiation (Bond et al., 2013; Hadley and Kirchstetter, 2012). The deposition of BC on snow and ice impacts the local and regional climate by altering solar radiation balance through snow albedo change and associated albedo positive feedback effects (Ramanathan and Carmichael, 2008; Flanner et al., 2007; Doherty et al., 2013; Qian et al., 2015; Schuckmann et al., 2016; Niu et al., 2017a). Recently, there has extensive studies been focused on BC and other light-absorbing impurities (e.g., dust, brown carbon (BrC), insoluble organic carbon (OC)) in the cryosphere and atmosphere because of their strong climate effects and radiative forcings (e.g., Kaspari et al., 2014; Li et al., 2017, 2018; Lee and Kim, 2010; Wang et al., 2015; Zhang et al., 2017, 2018; Kang et al., 2019). Those impurity particles, primarily denotes insoluble light-absorbing impurities (abbreviated as ILAIs), significantly contribute to snow and glacier melt through various mechanisms, such as snow albedo decrease and atmospheric warming caused by BC and other agents/particles. BC has been demonstrated to be the third most important agent in climatology behind carbon dioxide (CO_2) and methane (CH_4) (IPCC, 2013),

* Corresponding author at: Donggang West Rd 320, Chengguan district, Lanzhou 730000, China.
E-mail address: niuhw@lzb.ac.cn (H. Niu).

https://doi.org/10.1016/j.atmosres.2020.105002
Received 29 January 2020; Received in revised form 28 March 2020; Accepted 14 April 2020
Available online 15 April 2020
0169-8095/

with the estimated gross global anthropogenic-emissions of 7500 Gg yr^{-1} (uncertainty interval 2000–29,000 Gg yr^{-1}) and global radiative forcing of approximately 1.1 W m^{-2} with large-uncertainty (0.17–2.1 W m^{-2}) (Bond et al., 2013; Jacobson, 2001; Gertler et al., 2016; Liu et al., 2017). Dust particles originates from both anthropogenic and natural sources, with anthropogenic activities which involve agriculture, road, building industry, deforestation, etc. (Tegen et al., 2004; Kaspari et al., 2015). Dust usually acts as efficient ice nuclei in the polar ice/glacier (Si et al., 2018) and potentially influences solar radiation (Bergin et al., 2017; Lee et al., 2013). Episodic deposition of mineral dust on alpine glaciers, much like BC decreases snow albedo and inevitably possess impacts on water resource availability for people residing downstream (Immerzeel et al., 2010) and meltwater runoff (Qian et al., 2015; Skiles and Painter, 2018; Zhang et al., 2018), and increase of snow melt in snow covered and glacierization areas (Jacobson, 2005; Kaspari et al., 2014; Lau et al., 2010).

In recent years, a growing number of studies have evaluated the effects of melt amplification of surface snow due to BC and OC deposition (Aamaas et al., 2011; Doherty et al., 2013; Xu et al., 2012), and particularly, examined their enrichment factors and scavenging efficiencies (Niu et al., 2017b; Li et al., 2017; Yang et al., 2015), as well as the vertical redistribution of BC (Flanner and Zender, 2006; Flanner et al., 2007; Skeie et al., 2011) resulted from post-depositional processes (e.g., sublimation, perturbation, infiltration, wind-driven drifting) during the snowmelt season. The absorption of solar radiation caused by ILAIs in snowpack facilitates snow grain size growth and induces an earlier spring ablation (Flanner et al., 2007; Lee et al., 2013; Niu et al., 2017b). A larger snow grain size would cause albedo reduction of surface snow at all wavelengths (Hadley and Kirchstetter, 2012; Warren and Wiscombe, 1980). Once snowpack starts to melt, ILAI concentrations enriched at the snow surface (mostly within 4 cm in depth) with BC and other impurities mixed inside (Conway et al., 1996; Doherty et al., 2010; Doherty et al., 2013), further darkening snow, transforming the absorbed energy into internal heat in snowpack, thus largely warming the snowpack and driving glacial melt (Flanner et al., 2007; Qian et al., 2015; Li et al., 2019). As snow melting progresses, impurities in snow cover may be scavenged downward by the meltwater to a specific depth, or left at the top of the snowpack, however, the detailed mechanism of physiochemical processes (i.e. the rate and processes of chemical changes (at the atomic level) in the snowpack due to the disturbance of chemical or physical factors) of ILAIs in snowpack is yet to be fully understood and is still a topic of active research.

The Tibetan Plateau, also named as “the Third Pole” (Yao et al., 2012), is one of the most isolated and remote regions in the world, which is an ideal and pristine research site for cryosphere and atmospheric environments (Fig. 1). Glaciers and their meltwater in the southeast of Tibetan Plateau (TP) play an important role in feeding downstream rivers (Immerzeel et al., 2010; Gertler et al., 2016) and snowmelt runoff (Lau et al., 2018; Qian et al., 2011), which significantly impact the availability of fresh water resources and even food security and livelihood of millions of residents living downstream of those rivers. Therefore, a comprehensive study/comprehend of a series of physicochemical related snow aging and post-depositional processes is indispensable for a successful estimate of BC concentrations in glaciers over the TP cryosphere (Xu et al., 2012; Ming et al., 2013; Ji, 2016; You et al., 2010), direct in-situ field observations and measurements of ILAIs in snow and ice on glaciers in this region are still scarce and very limited due to its harsh environment and severe logistic difficulties.

This study based on extensive field observations and measurements of ILAI concentrations in snow/ice from four glaciers on the TP, combing with modeled atmospheric ILAIs at surface over the four glaciers in 2014 and 2015 using updated atmospheric chemical model, to robustly evaluate model performance, post-depositional processes of ILAIs in snow/ice, spatio-temporal pattern of ILAIs, optical properties of BC in snowpack, as well as chemical composition and morphology of individual particles in glacier cryoconite, and tentatively propose possible schemes for the parameterization improvement and optimization of atmospheric chemistry models.

2. Regional setting

The TP is the highest plateau in the world, with an area of over 3.6 million km^2 and the mean altitude of above 2500 m a.s.l. (Zhang et al., 2014). Numerous mountain glaciers are widely distributed on the TP. The southeast TP has two seasons: the rainy or monsoon season (June–September) and the non-monsoon season (October–May) (Niu et al., 2014; Niu et al., 2016; Niu et al., 2018; Li et al., 2015, 2016), its climate also has seasonal variations, i.e., the mean temperature in the monsoon season is higher than that in the non-monsoon season; large amount of annual rainfalls (more than 80%) occur during the monsoon season. Largely, the seasonal pattern of temperatures at four glacier sites (see below) on the TP is similar.

Mt. Yulong (26°59′-27°17′ N, 100°04′-100°15′ E) in the southeast TP, is also located in the transition region of altitude in China between the first level and the second level, and in the joint zone of a three-river fold system, the Songpan-Ganzi fold system. Sandstone and limestone are the main lithologies in the Mt. Yulong region. Baishui glacier (27°06′16″ N; 100°11′44″ E) is a typical temperate glacier on Mt. Yulong that generally has higher energy/heat fluxes compared with continental glaciers in the northern TP, especially at lower elevations of the snow-covered and/or glacierized areas. The length and the area of Baishui glacier is 1.90 km and 1.32 km^2, respectively. The height of the balance line of Baishui glacier is 4850 m, and the glacial melting rate is 9.20–9.90 cm d^{-1} during the ablation period (mainly in Jun.-Sep). The climate of Mt. Yulong is affected by multiple circulation systems, such as the South Asian monsoon, plateau monsoon, and westerly wind. Winter in Mt. Yulong is mainly controlled by the westerly circulation, forming a dry climate with little rainfall; during the summer monsoon, the warm and humid air from the Indian Ocean in the southwest is blocked by the Hengduan Mountains, and then the air mass detours from the southeast and arrives at Mt. Yulong. Annual precipitation in the Mt. Yulong exceeds 2000 mm. Zhadang (ZD) glacier (30°28′ N, 90°38′ E) lies in the southern TP, with its length of 1.8 km, area of 2.58 km^2 and the highest elevation of 5980 m a.s.l.. Based on the physical properties of this glacier, it can be classified as a continental glacier. Recent study has shown that the terminal of the ZD glacier is shrinking with a rate of 10.0 m yr^{-1} (Li et al., 2018). Xiaodongkemadi (XDKMD or XDK) glacier (33°04′ N, 92°04′ E) located on Mountain Tanggula, in the central of TP, is a typical continental and valley glacier, with the average atmospheric temperature above 0 °C during June–September each year and large amount of rainfall occurs at this period (Li et al., 2017). The area of XDK glacier is about 1.6 km^2 and its mean elevation is approximately 5500 m asl. Laohugou (LHG) glacier (39°30′ N, 96°32′ E) located at the west of Qilian Mountain, and the northern edge of TP. There are many continental glaciers in Qilian Mountain and they have been experiencing rapid retreat during the last 50 years (Wang et al., 2011). LHG No. 12 glacier is one of the largest valley glaciers on Qilian Mountain, which has an area of 21.9 km^2. The terminal elevation of LHG No. 12 is 4260 m asl.

3. Materials and methods

3.1. In-situ snow sampling

The measured ILAI data used in this work was absolutely based on extensive field observations and sample collection during the pre-monsoon (e.g., April, May) or spring and monsoon season (Jun.-Sep.) in 2015, 2016, 2017, and 2018 (Table S1). The measured samples primarily include snowpit samples and surface aged-snow samples from Baishui glacier on Mt. Yulong and other three glaciers (ZD, DKMD, LHG) on the TP. Snowpits were excavated consecutively during each

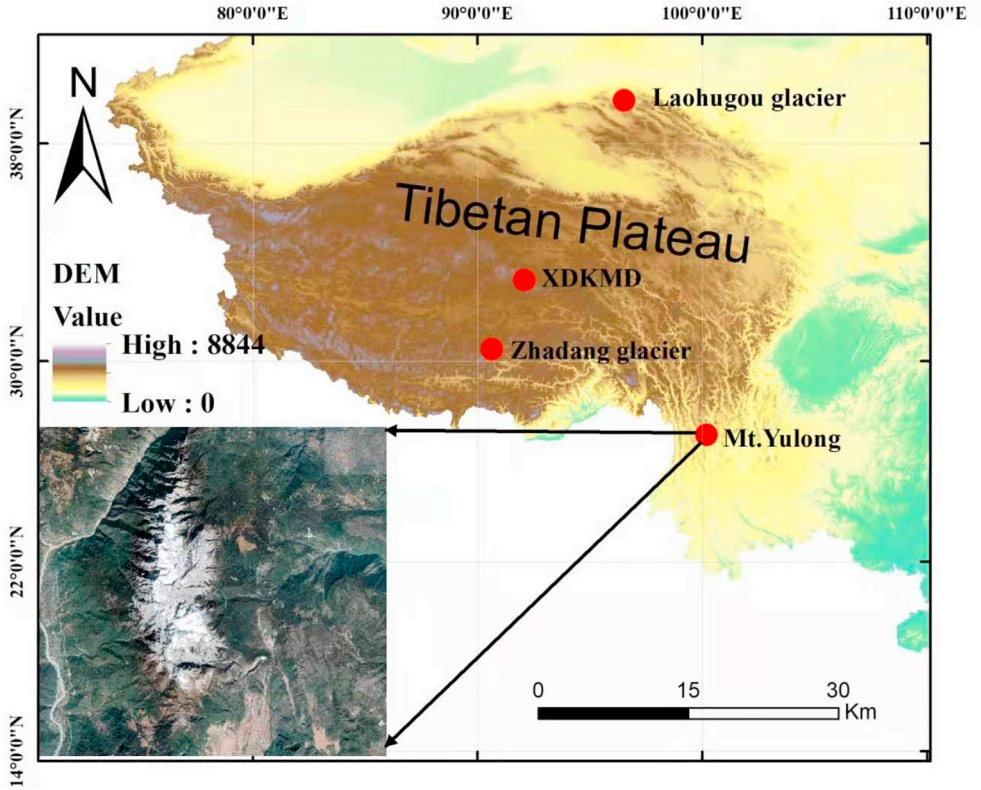

Fig. 1. The location of Mt. Yulong, Laohugou (LHG), Xiaodongkemadi (XDKMD), and Zhadang (ZD) glaciers on the Tibetan Plateau.

field campaign of 2015–2018, mostly at the same site (27°06′16.3″ N; 100°11′44.4″ E) at an altitude of 4700 m asl. Snowpit samples were collected continuously at an interval of 10 cm from the top to the bottom of snowpit profiles, snow samples were collected immediately each time after the pit was dug. Finally, 13 snowpits and 190 snowpit samples were measured and used in this study. Surface aged-snow samples (about 7 cm in depth on glacier surface) were collected broadly from multiple elevations (in the range of 4600–4780 m asl) of Baishui glacier in the spring season in 2015–2018. In addition, cryoconite samples were collected according to elevation gradient (50 m) on Baishui glacier during field campaigns. A total of 160 surface aged-snow samples were analyzed in this study. The maximum depth/thickness of snowpit that occurred in the early spring season in Mt. Yulong was nearly 3.5 m.

All the samples were packed in Whirl-Pak® bags (500 ml in capacity) and filtrated immediately after melting at ambient temperature. The melted samples were evenly shaken before they were filtered through the pre-baked quartz filters (baked earlier for 6 h at 550 °C) (Whatman® quartz filter, 47 mm in diameter) using a vacuum pump. Afterwards, the filtered samples were wrapped in aluminium foil and kept frozen, and then transported to the State Key Laboratory of Cryospheric Science in Lanzhou for the final lab analysis. The sampling glass bottles, and mini snow shovels were baked prior to they were used in sample collection to avoid possible contamination to snow samples. The analysis method of ILAIs and other relevant measurements are provided in the supplementary material. Snow OC and BC on the quartz filters were measured using a Desert Research Institute (DRI) Model 2001 Thermal/Optical reflectance Carbon Analyzer (Atmoslytic Inc., Calabasas, California). Accurate measurement of ILAIs concentrations in snow is crucial for the assessment of their climatic impacts. Actually, there are some biases in the measurement of BC and OC in snow, using a thermal-optical transmittance method. This method can cause the underestimation of BC concentrations in snow because the efficiency of the quartz fiber filter decreases with decreasing BC diameter. On the other hand, the thermal-optical method causes the overestimation of BC concentrations partly due to pyrolyzation of some OC in snow samples during the initial heating steps, and finally the pyrolyzed OC was determined as BC due to BC-like light absorption (Lim et al., 2014). In addition, dust concentrations in snow samples were measured using a gravimetric approach by weighing the dried quartz fiber membranes with a high precision scale (Liangping-FA2004, uncertainty: 0.1 mg) to get the mass difference before and after the filtration of snow samples.

3.2. WRF-Chem model

A fully online meteorology-chemistry model (WRF-Chem), updated by PNNL scientists, is used to conduct multiyear quasi-global simulations with 360 × 145 grid cells (180° W–180° E, 67.5° S–77.5° N) at 1° horizontal resolution. The simulation is configured with 35 vertical layers up to 50 hPa. For model physics, we used a set of selected schemes including the Noah land surface scheme, MYJ (Mellor–Yamada–Janjic) planetary boundary layer scheme, Kain–Fritsch cumulus scheme, Morrison 2-moment microphysics scheme, and RRTMG longwave and shortwave radiation schemes. National Center for Environmental Prediction final analysis (NCEP/FNL) data at 1° horizontal resolution and 6 h temporal intervals is used for the meteorological initial and lateral meridional boundary condition as well as for nudging u and v winds every 6 h. Periodic boundary conditions in the zonal direction are employed.

We used the MOSAIC (Model for Simulation Aerosol Interactions and Chemistry) aerosol module (Zaveri et al., 2008) coupled with the CBM-Z (carbon bond mechanism) photochemical mechanism (Zaveri and Peters, 1999) for aerosol simulation in this study. The MOSAIC aerosol scheme includes physical and chemical processes of nucleation, condensation, coagulation, aqueous phase chemistry, and water uptake by aerosols and simulates all major aerosol components in eight size bins. The details of these aerosol process parameterizations are provided in Zhao et al. (2013a). REanalysis of the TROpospheric (RETRO) chemical composition inventories (Schultz et al., 2007) is used for

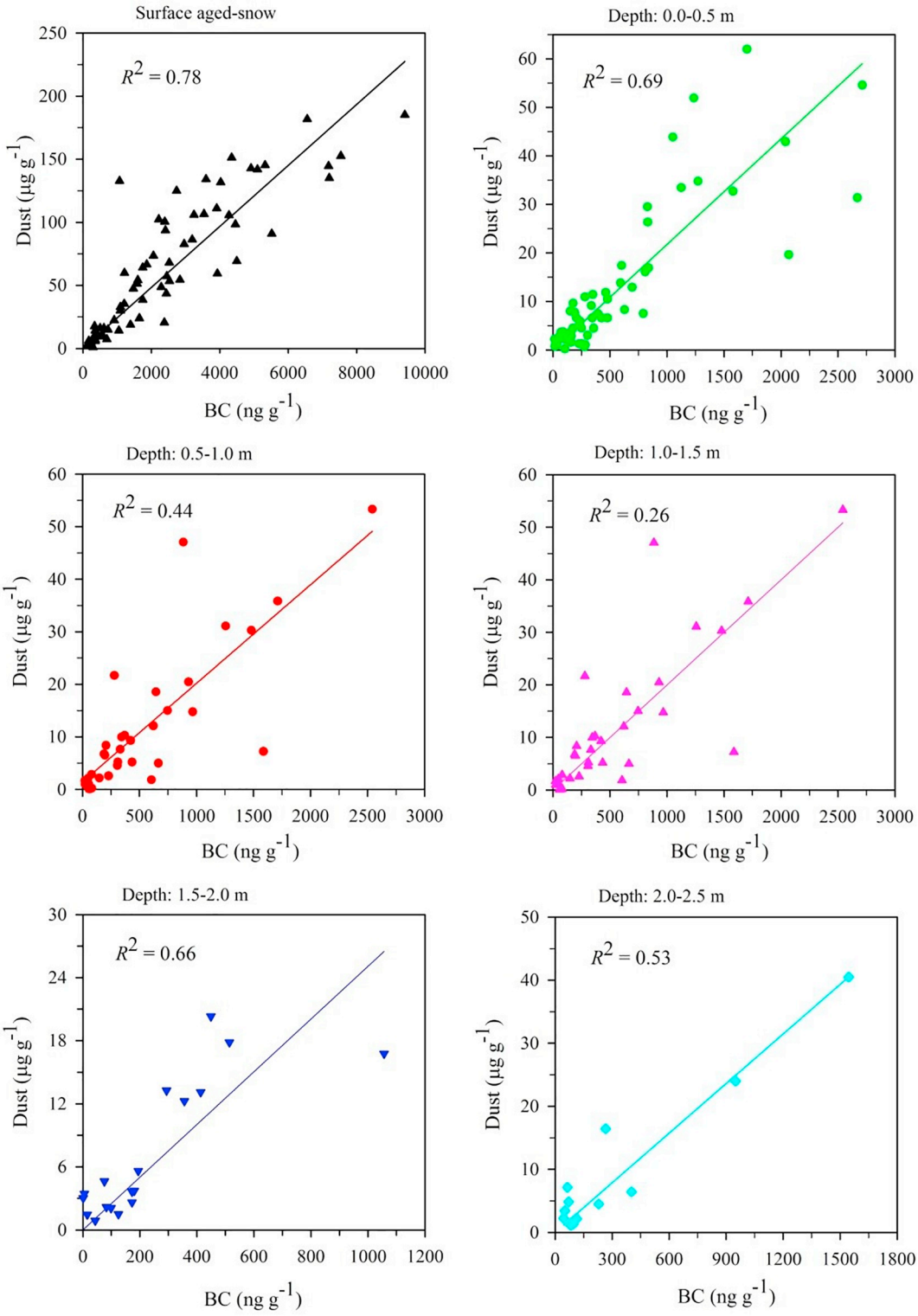

Fig. 2. Correlations between measured BC, dust concentrations in surface aged-snow and five depth bins of snowpit from Mt. Yulong.

anthropogenic emission fluxes globally; except over East Asia and the United States. China emission inventory for 2010 described by Lu et al. (2011) at a 0.1° × 0.1° horizontal spatial resolution and a monthly temporal resolution for the simulation period is used over China for BC, organic matter (OM), and sulfate emissions in the simulations. The Asian emission inventory described by Zhang et al. (2009) at 0.5° × 0.5° horizontal resolution for 2006 is used for other particulate emissions over remaining regions of East Asia. Anthropogenic emissions from the National Emission Inventory (NEI) 2011 are used over USA. Biogenic emissions are calculated following Guenther et al. (1994). Biomass burning emissions are obtained from the Global Fire Emissions Database, version 3 (GFEDv3) and updated every day. Sea-salt emission follows Zhao et al. (2013b). Goddard Chemical Aerosol Radiation Transport (GOCART) dust emission scheme (Ginoux et al., 2001) is used to calculate dust emissions. The simulated meteorology and detailed 3-D aerosol distribution over Asia are evaluated with various reanalysis

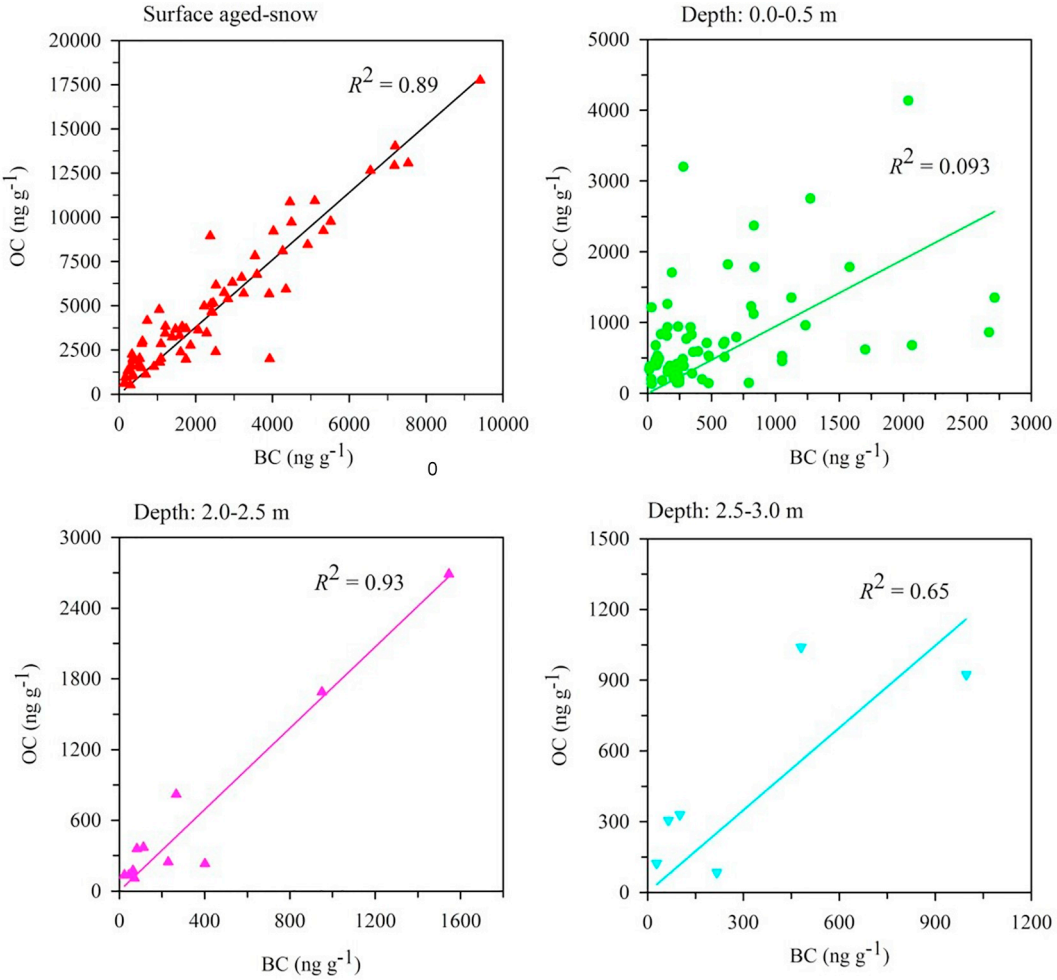

Fig. 3. Regression analyses between measured BC, OC concentrations in surface aged-snow and three depth bins of snowpit from Mt. Yulong.

and observational data sets (Hu et al., 2016; Sarangi et al., 2019). Three-hourly, simulated surface concentrations of BC, OC and dust in atmospheric aerosol from this Quasi-global channel WRF-Chem simulation are used for analysis over the four study sites (100° E, 90° E, 92° E, 96° E and 27° N, 30° N, 33° N, 39° N; 4700 m, 5750 m, 5600 m, 4137 m) during summer season (May to August) of 2014 and 2015.

3.3. CALIPSO detects of aerosol

The Cloud-Aerosol Lidar and Infrared Pathfinder Satellite Observation (CALIPSO) satellite measures global aerosol profile data. CALIPSO offers the global measurement of the three-dimensional distribution of aerosol (Niu et al., 2019). It has a series of 16-day orbit repeat-cycle (Ziskin, 2016). The CALIOP data set has been gridded in a 3-D grid of 1° latitude × 1° longitude × 200 m altitude in this study. The particulate depolarization ratio (from the 532 nm channel) and aerosol extinction coefficient at 1064 nm are used to investigate vertical distribution and structure of aerosol and/or aerosol layer over this region.

4. Results and discussion

4.1. The correlation of ILAI concentrations in snowpit and surface snow

Correlation analysis between measured BC and dust in snowpit was extensively conducted. The results indicated that there exist strong relations between BC and dust (R^2 = 0.78, p < .05) (Fig. 2). This finding suggests that BC and dust in surface snowpack are closely co-existed, probably by/in the forms of internally or externally mixed, which is largely associated with snow/firn grain metamorphism and densification (e.g., Bond et al., 2006; Cappa et al., 2012; Dang et al., 2016; Liou et al., 2014). To evaluate the evolution of BC and dust concentrations, and their physiochemical processes in snowpack, we further performed a detailed regression analysis of BC and dust concentrations in vertical profiles of snowpack. The whole profile of each snowpit was divided into several depth bins at an interval of 50 cm and correlation of BC and dust in each depth bin were investigated step by step. Because the depth of snowpits was mostly less than 3 m, so we only statistically processed data for snowpits within 3 m. It is noticeable that the correlation between BC and dust varied with increasing depth of snowpit (Fig. 2); R^2 = 0.69 (for 0.0–0.5 m depth), R^2 = 0.66 (1.5–2.0 m), R^2 = 0.53 (2.0–2.5 m), while the lowest correlation coefficient value (R^2 = 0.26) was obtained for 1.0–1.5 m depth which suggests the leaching and percolation processes (e.g., Wipf et al., 2015; Tranter et al., 1992; Xu et al., 2009) might have played a discernable role in snowpit when its depth is deeper than 1.5 m. Generally, BC is emitted from anthropogenic sources, while dust particles are emitted from anthropogenic and natural sources. Moreover, the sizes of dust particles are larger than BC particles, which can be efficiently removed by dry deposition. Taking these factors into account, poor correlations between BC and dust in snow layer are caused by not only leaching and percolation processes, but also the differences of their sources and deposition processes (wet and dry processes). Therefore, evolution of the correlation between BC and dust in vertical snowpack during the snowmelt season actually cannot be revealed by prevalent atmospheric models. The difference in the extent of correlation between BC and dust

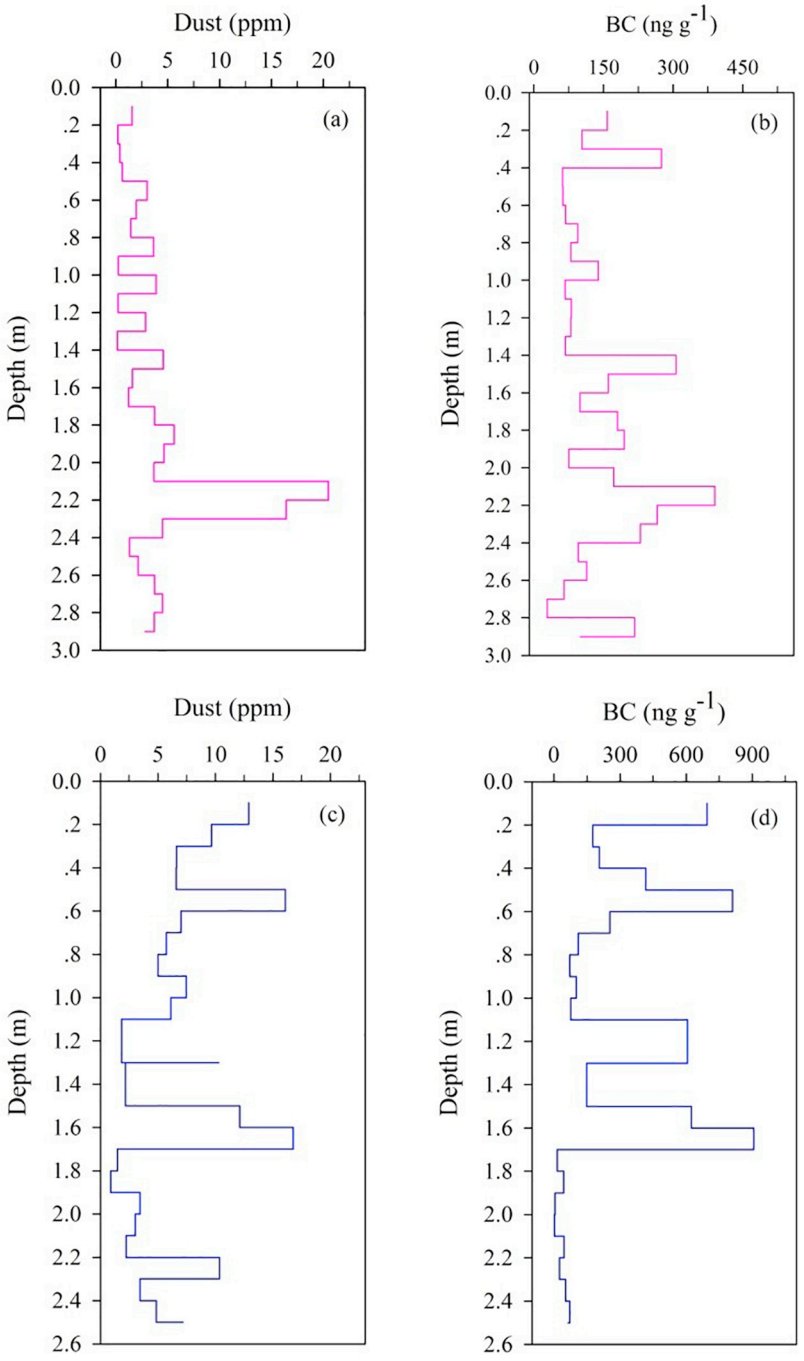

Fig. 4. Vertical distribution of BC and dust in snowpits collected on 14 June 2017 (a, b) and 22 June 2017 (c, d).

was primarily due to their different water solubilities and scavenging efficiencies (by the snowmelt). Besides the correlation between BC and dust in diverse snow samples, we conducted regression analyses for BC and OC in surface aged-snow and snowpits. Results revealed that there is apparent difference between the extents of correlation of BC-OC in surface aged-snow and in snowpits. BC and OC in surface aged-snow have strong correlation with coefficient $R^2 = 0.89$ (Fig. 3), similar with correlation between BC and dust found in surface aged-snow. High correlation between BC and OC in surface aged-snow of glaciers reflects their common emission-sources (Wang et al., 2015; Niu et al., 2017b). However, for snowpit samples, correlation between BC and OC varied significantly in different depth bins/intervals. In contrast to the observed correlation between BC and dust in snowpits, the correlation between BC and OC in vertical snowpit is very weak when the depth of snowpit less than 2.0 m. At the same time, the correlation between BC and OC is even as strong as found in surface aged-snow ($R^2 = 0.89$, $p < .01$) for snowpit samples at 2.0–2.5 m and 2.5–3.0 m depth intervals (Fig. 3). This is an interesting and novel finding, which clearly manifests the evolution of correlation between BC and OC in the profile of snowpits, and indirectly reveals the physiochemical processes of BC and OC in snowpit. Therefore, combing with correlation analysis of BC, dust, and OC in snowpack, it is notable that at the bottom/lower fractions of snowpits, there exist strong correlations between BC and dust, BC and OC, which were probably resulted from a series of post-depositional processes in snowpits, such as extensive leaching, percolation, and meltwater scavenging effects during the snow melting season; while also partially indicating about their common source in snowpack. Moreover, previous studies demonstrated that the scavenging

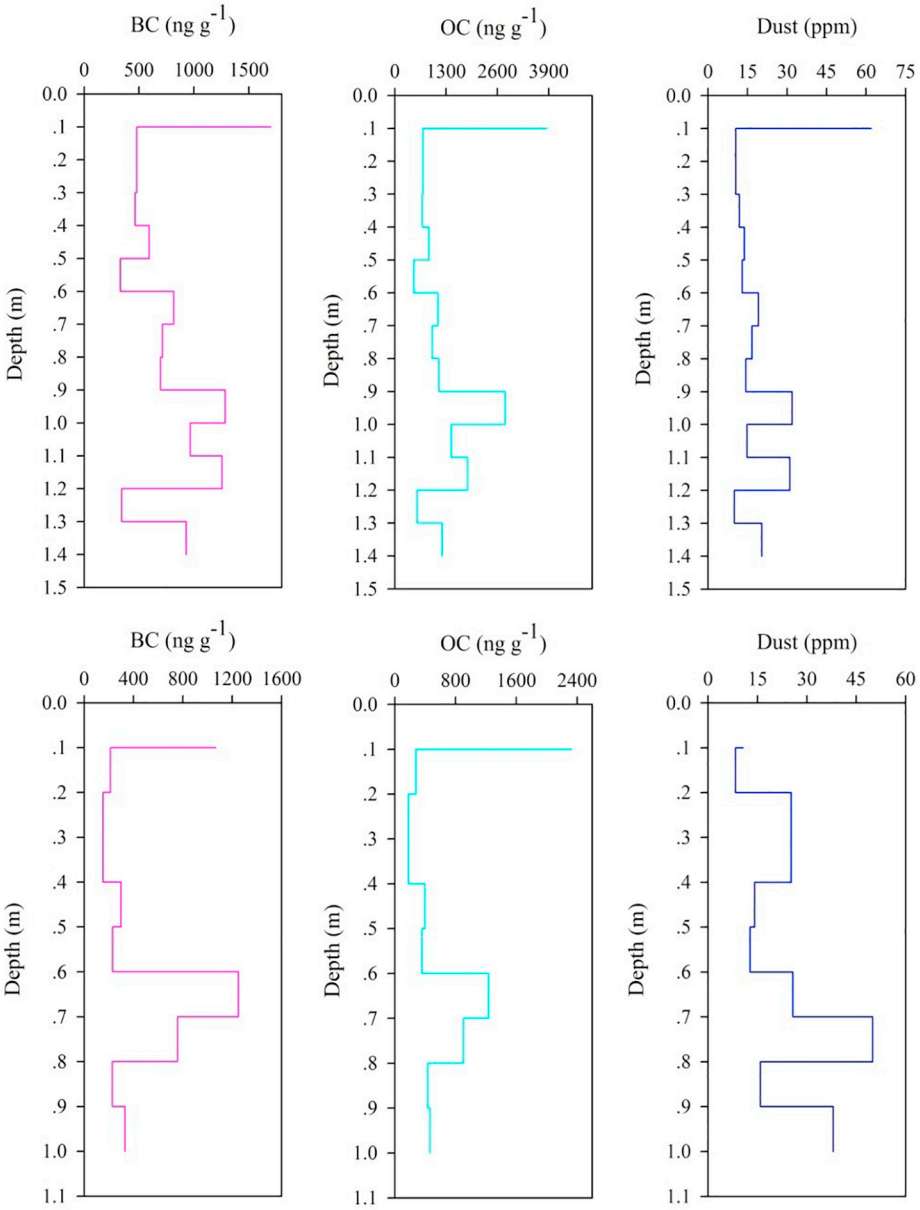

Fig. 5. Vertical distribution of BC, dust, and OC concentrations in snowpits collected on 3 June 2016 (upper panel) and 17 April 2018 (lower panel) from Mt. Yulong.

efficiencies of BC and OC in vertical snowpack are closely associated with their hydrophilicity (e.g., Doherty et al., 2010; Niu et al., 2017b). It is important to understand the re-distribution of ILAI particles into the snowpack by physiochemical processes and post-depositional process. Based on field observations, the surface temperature of snowpack on Mt. Yulong has been measured for several times during the sampling campaign (mostly in May–June), the average surface temperature of snowpack was 0.26 ± 0.18 °C (Table S2). Thus, the surface snow melts and physiochemical processes and post-depositional processes might be occuring, and the re-distribution of ILAI particles in the snowpack was dominated by extensive snow melting.

In addition, vertical distribution of BC and dust in snowpit has been performed and the results are shown in Fig. 4. By taking the profile of each snowpit as a unity, the concentration of impurities in snowpit consecutively distributed along the vertical profile. As demonstrated in Fig. 4, the profile of BC and dust concentrations in snowpit is consistent with each other, particularly, the high and low values of BC and dust resultant of the enrichment and scavenging effects are in phase. Similar results can also be found in snowpit sampled in May and June 2016 (Fig. S1). Therefore, strong correlation between BC and dust in snowpit (showed in Fig. 2) can be further verified by their vertical distribution. The robust correlations and consistent profiles between BC and dust emphasize their common origin sources or similar post-depositional enrichment and scavenging/leaching processes in snowpit. Exceptional high BC and dust contents in snowpit at depths of 1.5 m and 2.2 m measured on 14 June 2017 (Fig. 4a, b), and 0.6 and 1.7 m measured on 22 June 2017 (Fig. 4c, d) might be result of dust/firn storm layers and/or the outcome of post-depositional enrichment effect.

The vertical distribution of BC, OC and dust concentrations was further investigated for snowpits excavated on 3 June 2016 and 17 April 2018. Results demonstrate that the relative change of those impurities along the profiles of snowpits is uniform (Fig. 5), their vertical distribution along the profiles of snowpits is nearly identical, which is somewhat different from the results of correlation and statistical analyses of ILAIs in different depth intervals of snowpit.

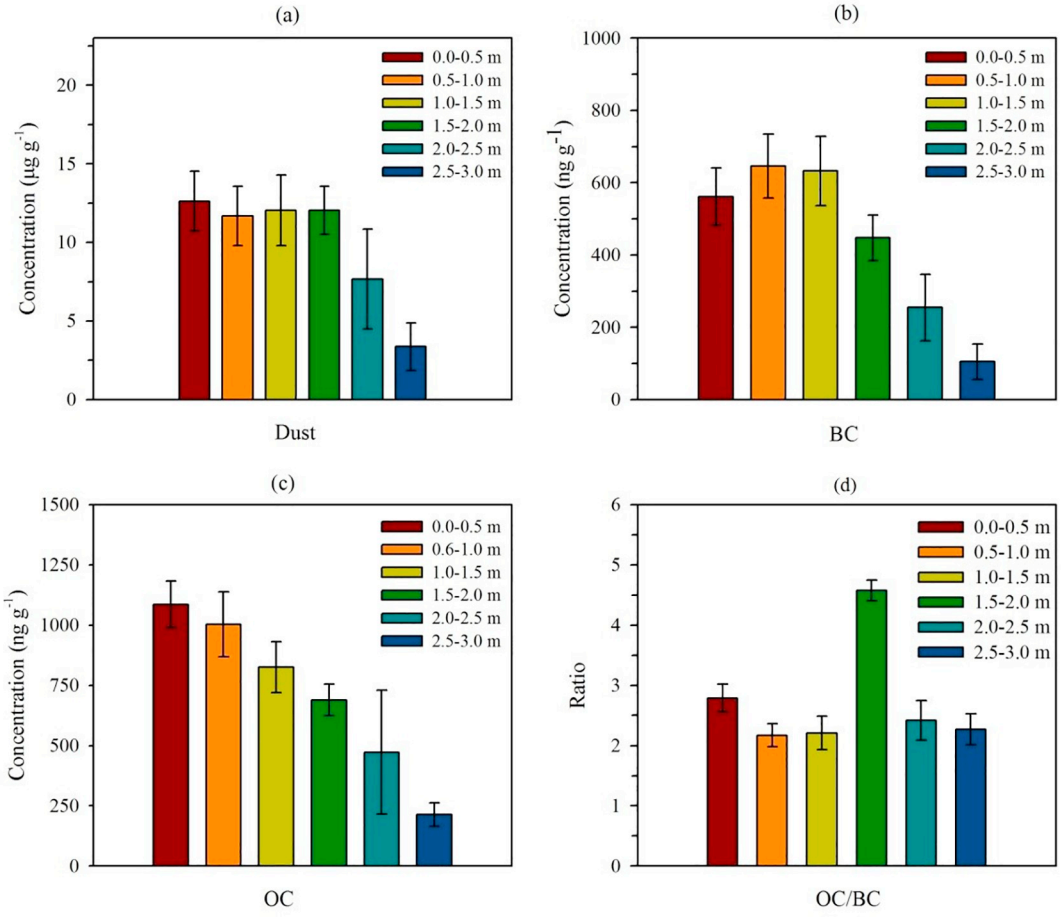

Fig. 6. The average BC, OC, dust concentrations and OC/BC ratio in different depth-intervals of snowpit from Mt. Yulong.

Table 1
Statistical results of multiple comparisons for BC concentrations in five depth-intervals of snowpit using LSD method.

(I)	(J)	Mean difference (I-J)	Std. error	Sig.	95% confidence interval	
					Lower bounder	Upper bounder
0.0–0.5 m	0.5–1.0	86.9481	214.796	0.687	−342.157	516.053
	1.0–1.5	341.171	214.796	0.117	−87.933	770.276
	1.5–2.0	**650.002***	214.796	0.004	220.897	1079.107
	2.0–2.5	**525.529***	218.888	0.019	88.249	962.808
0.5–1.0	0.0–0.5	−86.948	214.796	0.687	−516.053	342.157
	1.0–1.5	254.223	214.796	0.241	−174.882	683.328
	1.5–2.0	**563.054***	214.796	0.011	133.949	992.159
	2.0–2.5	**438.581***	218.888	0.039	1.301	875.859
1.0–1.5	0.0–0.5	−341.171	214.796	0.117	−770.276	87.933
	0.5–1.0	−254.223	214.796	0.241	−683.328	174.882
	1.5–2.0	308.831	214.796	0.155	−120.274	737.936
	2.0–2.5	184.357	218.888	0.403	−252.922	621.636
1.5–2.0	0.0–0.5	**−650.002***	214.796	0.004	−1079.107	−220.897
	0.5–1.0	**−563.054***	214.796	0.011	−992.159	−133.949
	1.0–1.5	−308.831	214.796	0.155	−737.936	120.274
	2.0–2.5	−124.473	218.888	0.572	−561.753	312.805
2.0–2.5	0.0–0.5	**−525.529***	218.888	0.019	−962.808	−88.249
	0.5–1.0	**−438.581***	218.888	0.049	−875.859	−1.301
	1.0–1.5	−184.357	218.888	0.403	−621.636	252.922
	1.5–2.0	124.474	218.888	0.572	−312.806	561.753

Bold indicates the mean difference is significant at the 0.05 level.
* The mean difference is significant at the 0.05 level.

4.2. Statistical analysis of ILAIs in snowpit

According to the correlation analysis of BC, dust, and OC in snowpit, their correlations were significantly varied with the depth of snowpit. In this section, statistical analysis of the average BC, OC, and dust concentrations in snowpit have been conducted. The average ILAI concentrations in surface aged-snow were almost five folds higher than those in snowpit, thus, in order to make it convenient for the

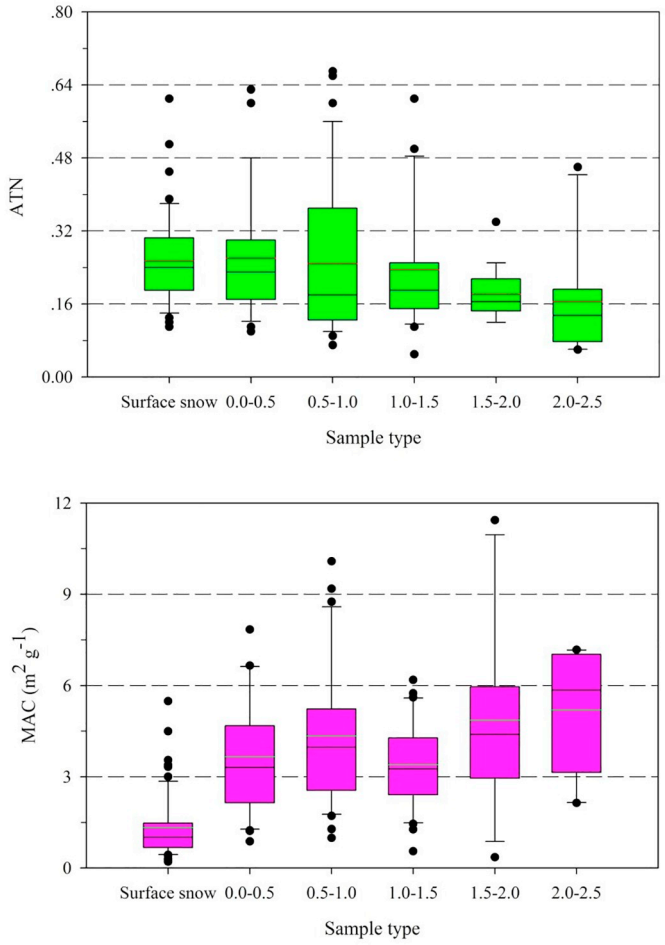

Fig. 7. Variation of light absorbing characteristics of BC in the surface aged-snow and five depth intervals of snowpit. ATN denotes optical attenuation of BC, MAC denotes mass absorption cross-section of BC (unit: $m^2\ g^{-1}$).

comparison, we only compare the average ILAI concentrations in six depth-intervals of snowpit as presented in Fig. 6. Statistical results show that the average dust concentrations sharply decreased in snowpit for the depth deeper than 2.0 m. At the bottom of snowpit (depth in the range of 2.5–3.0 m), snowpit samples have the lowest average impurity concentration (Fig. 6a, b, c). The average BC concentrations in six depth intervals were dynamically varied; higher BC concentrations were detected in depth intervals of 0.5–1.0 m and 1.0–1.5 m in snowpit, which might be due to post-depositional enrichment processes. However, below the depth of 1.5 m, BC concentrations significantly decreased. Mean OC concentrations consecutively decreased from top to bottom of snowpits because of strong melt-scavenging effect. In addition, photolysis effect of dissolved OC in snowmelt causes considerable decrease of OC contents in snowpit during the snow melting season (Anderson et al., 2008; Molot and Dillon, 1997; Niu et al., 2017b). The ratio of OC to BC (OC/BC) in snowpit nearly has no apparent variation, its highest value was found in snow samples of 1.5–2.0 m interval in snowpit (Fig. 6d). The OC/BC ratio in snowpit was significantly lower than that in surface aged-snow (3.61 ± 0.28) on Mt. Yulong, this can be attributed to different melt strengths of surface snow and snowpit samples as well as different water-solubilities (and/or enrichment, melt-scavenging efficiencies) of BC and OC. Moreover, the ILAI concentrations in snow are also strongly influenced by their transport, precipitation amount, and deposition process, which might pose positive effects on the characteristics of ILAIs in six-depth intervals of snowpit. However, there is no quantitative information on these processes currently. Extensive in-situ field observations and measurements over the mountain glaciers are needed to get more robust conclusions.

To make sure whether significant difference exists in between BC, OC and dust concentrations at different intervals of snowpit, plentiful research and statistical analysis have been specifically conducted in this sub-section. Results indicate that BC concentrations in snowpit samples of five depth intervals were significantly different (Table S3). Particularly, significant difference of BC concentrations was found between depth intervals of 0.0–0.5 m and 1.5–2.0 m ($p = .004$), between 0.0 and 0.5 m and 2.0–2.5 m ($p = .019$). For BC concentrations in snowpit samples of 0.5–1.0 m depth interval, there was significant difference with those of 1.5–2.0 m ($p = .011$) and 2.0–2.5 m ($p = .039$) (Table 1). However, no significant difference among five depth intervals was found for dust concentrations in snowpit by statistical ANOVA method (Table S4). Statistical results of multiple comparisons for dust concentrations in five depth intervals of snowpit are shown in Table S5. Moreover, OC concentrations in snowpit of different depth intervals have significant difference ($p = .04$) as demonstrated in Table S6. Multiple comparisons for OC concentrations in five depth intervals of snowpit have been conducted to further investigate significant difference among depth intervals. Results show that the mean difference of OC concentrations between depth intervals of 0.0–0.5 m and 1.5–2.0 m ($p = .012$), 0.0–0.5 m and 2.0–2.5 m ($p = .046$) was significant (Table S7), respectively. In addition, between depth intervals of 0.5–1.0 m and 1.5–2.0 m of snowpit, OC concentrations were significantly different ($p = .015$). Therefore, discrepancies in significant difference of BC and OC, and dust concentrations among different depth intervals reflect their different hydrophilicities, physiochemical properties, and post-depositional processes in snowpit.

4.3. Changes in optical properties of BC in vertical snowpack

The absorption signal of thermal EC (also termed as BC) can be reflected by optical-attenuation (ATN), based on the transmittance signal during the filter measurement. Compared with the ATN of blank filter (0.00 ± 0.01) (Cheng et al., 2011), the derived ATN value of particle-loaded filter is usually attributed to the existence of BC particles. The mass absorption cross-section (MAC) of BC is calculated through the ATN and the amount of EC loaded on the quartz filter, the uncertainty in estimating MAC was ±7%. Detailed information on ATN and BC MAC is given in the Supplementary Information. ATN and MAC of BC have been statistically determined for surface aged-snow and snowpit samples. Results indicate that from the surface to the bottom of snowpit, ATN values were gradually decreased vertically with depth. Surface aged-snow has the highest ATN value (0.25 ± 0.012), whereas snow samples from the bottom of snowpit (2.0–2.5 m) have the lowest ATN value (0.16 ± 0.018) (Fig. 7). However, for MAC of BC, it increased with depth increment from the surface to the bottom of snowpit. Snow samples of 2.0–2.5 depth interval have the highest BC MAC value (5.20 ± 1.05 $m^2\ g^{-1}$). Thus, the trend of BC MAC throughout the profile of snowpit is opposite to that of ATN in snowpack. This is an interesting scientific phenomenon which reflects the variation of optical properties of BC in snowpack/snowpit. Lower BC MAC values detected in surface aged-snow are probably due to strong photo-chemical reactions (one of the post-depositional processes), which is caused by the absorption of photons by BC molecules, when BC was exposed at the surface of glaciers during glacier ablation season (Mopper and Kieber, 2002). Variations of the optical properties of BC in vertical snowpack might have occurred due to the different melt strengths of snowpack at various depths. In addition, external coating by non-carbon components (e.g., dust, sulphate, and nitrate) can enhance BC MAC which can be termed as absorption amplification/enhancement (e.g., Schnaiter et al., 2005; Knox et al., 2009; Niu et al., 2018). The extent of internal-mixing of BC with other species can also affect BC MAC value (Cappa et al., 2012; Jacobson, 2001). BC MAC is an important parameter for predicting climate forcing of BC-in-snow. The findings of this study indicate that current estimations of climate

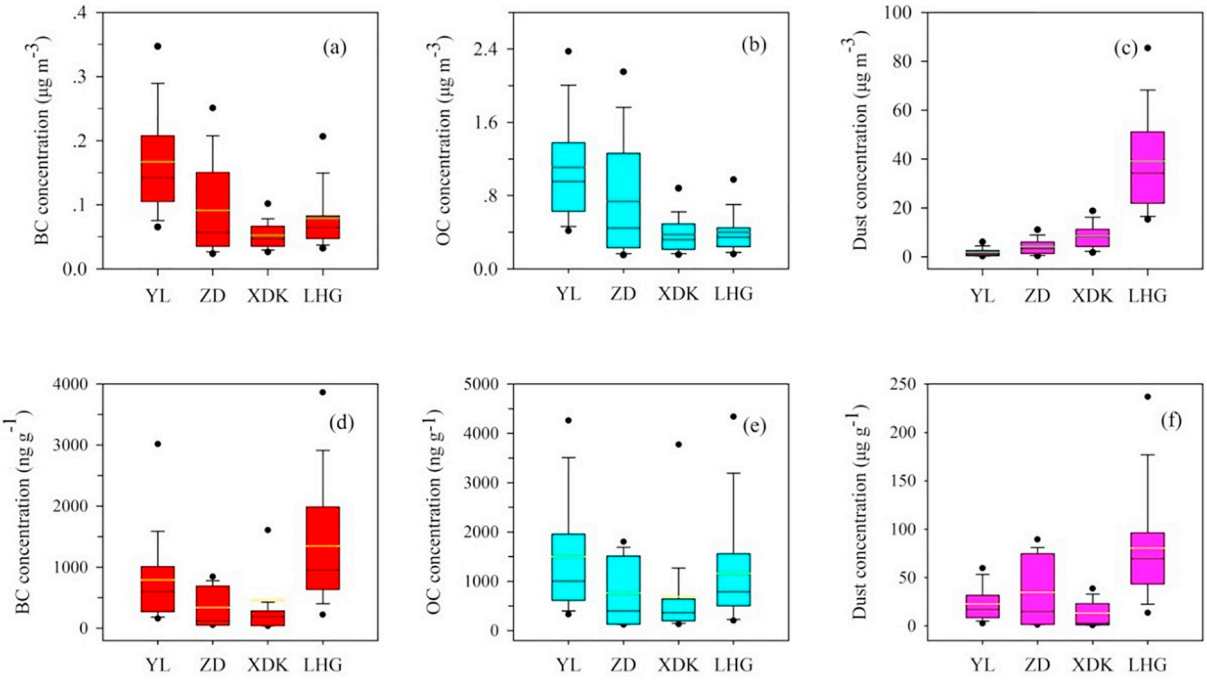

Fig. 8. Spatial difference of ILAIs concentrations in atmospheric aerosol at surface over the four glaciers (a, b, c) and in the surface-aged snow of glaciers (d, e, f) on the TP. The average ILAI contents in surface-aged snow of ZD glacier (Li et al., 2018), XDKMD glacier (Li et al., 2017), LHG glacier (Zhang et al., 2017), and Baishui glacier on Mt. Yulong (YL) are presented in the figure.

forcing induced by BC might be overestimated because usually larger BC MAC value (7.5 m^2 g^{-1}) is employed in radiative transfer models (e.g., Aoki et al., 1999; Nordmann et al., 2013; Jacobi et al., 2015). The multiple variations of ATN and MAC in vertical profile of snowpack suggest it is necessary for a proper parameterization/optimization of light absorption property of BC, particularly in estimating BC radiative forcing on a regional/global scale.

4.4. Spatial and annual difference of ILAIs in snow of glaciers

Based on simulated and measured ILAI concentrations in atmospheric aerosol and surface-aged snow, spatial difference of ILAIs in snow and atmospheric aerosol over the four glaciers on the TP has been performed. Results indicate that BC and OC concentrations of atmospheric aerosol over the surface of the four glaciers are sharply decreased from the south (Mt. Yulong) to the north (LHG glacier) of the TP (Fig. 8a, b). Whereas atmospheric dust concentrations over the surface of glaciers are rapidly increased from the south to the north of the TP, this is relatively easy to comprehend because glaciers located in the north of the TP, are close to arid or semi-arid regions, where are well-known as dust source regions. Additionally, the measured ILAI concentrations in surface aged-snow over the measurement locations (Fig. 8d, e, f) present distinct spatial pattern, which is consistent with the pattern derived from the modeled results (Fig. 8a, b, c). The spatial distribution of ILAI contents in surface-aged snow show that LHG glacier has the highest BC, OC, and dust concentration among the four investigated glaciers, followed by high BC and OC contents in snow of Yulong glacier. Deposition of atmospheric pollutants from local anthropogenic activities at Mt. Yulong and long-range transport from south Asia account for relatively high impurity contents in surface-aged snow on Mt. Yulong.

Simulated Atmospheric BC, dust and OC concentrations at surface over the four glaciers in May–August 2014 and 2015 have been employed to investigate monthly variation and annual difference. Statistical results show that from May to August, concentrations of ILAIs were significantly decreased both in 2014 and 2015 (Fig. 9). Atmospheric aerosol at surface over the Mt. Yulong in May 2014 and 2015 has the highest ILAI concentration and sharply decreased in June, whereas from June to August, ILAI concentrations were gradually decreased, in August snow samples nearly have the lowest ILAI concentration, especially in 2014. Monthly variations of atmospheric BC, OC, and dust concentrations at surface over the four glaciers were consistent with each other either in 2014 or in 2015. Additionally, monthly variation of atmospheric ILAIs at surface over ZD, DKMD, and LHG glaciers has also been investigated. Compared to monthly trend of ILAIs at Mt. Yulong, similar monthly variation of ILAIs can be detected at DKMD glacier (Fig. S2) and ZD glacier (Fig. S3), i.e., ILAI concentrations have been significantly decreasing from May to August both in 2014 and in 2015. However, monthly variation of atmospheric ILAIs at surface over LHG glacier was different from that over Mt. Yulong and the other two glaciers (Fig. S4). There was no decreasing trend of atmospheric ILAI contents from May to August at surface over the LHG glacier, except dust content. This phenomenon indicates that the seasonality of ILAIs in atmosphere at surface over the glaciers on the TP is characterized by distinct spatial heterogeneity, particularly for those glaciers located in the south and north of the TP. Numerous factors can interpret this phenomenon, such as the geo-location, topography, precipitation, as well as the intensity of local anthropogenic activities, etc. Furthermore, atmospheric ILAI concentrations at surface over the glaciers in May–August 2015 were apparently higher than those in 2014 (Figs. 9, S2, S3), which suggests much stronger deposition of carbonaceous aerosol and/or airborne dust particles in 2014 on snow/ice of glaciers over the TP, probably because of annual changes in emission sources of carbonaceous aerosol and/or annual changes in the contribution of diverse emission divisions or sources (Wang et al., 2015).

With the purpose of evaluating model performance in simulating impurities deposited in snow and ice, regression analysis between simulated values and measured concentrations of ILAI in atmospheric aerosol at surface and snow from Mt. Yulong and LHG glacier No. 12 has been conducted. Results presented in Fig. 10 show that there exists strong correlation between simulated and measured BC concentrations (R^2 = 0.78), as well as between simulated and measured OC

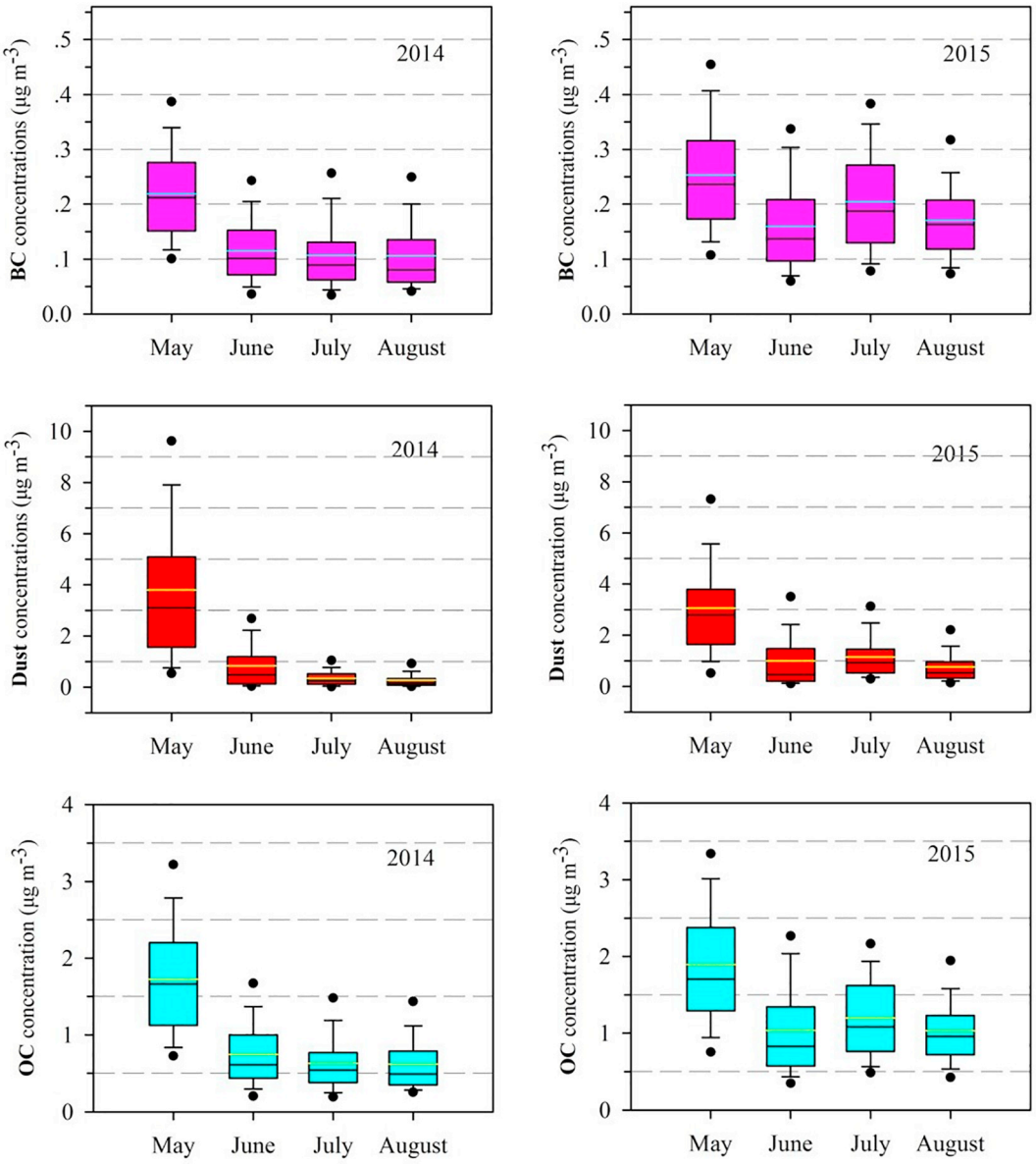

Fig. 9. Monthly and annual differences of the modeled BC, dust, and OC concentrations in aerosol at surface over Mt. Yulong in May–August in 2014 and 2015.

concentrations (R^2 = 0.67) in surface snow on Mt. Yulong. However, correlation between simulated and measured dust concentrations (R^2 = 0.39) was not as strong as those of BC and OC. The modeled atmospheric ILAI concentrations were underestimated. For example, the measured average BC and OC concentrations in Mt. Yulong aerosol were 1.51 ± 0.93 and 2.57 ± 1.32 μg m^{-3}, respectively (Niu et al., 2018), which significantly higher than modeled BC (0.17 ± 0.01 μg m^{-3}) and OC (1.11 ± 0.41 μg m^{-3}) concentrations of atmospheric aerosol over this region. Regarding LHG glacier, close correlation is found between measured and modeled BC concentrations (R^2 = 0.56) and OC concentrations (R^2 = 0.64) (Fig. 10). However, correlation between measured and modeled dust concentrations in LHG glacier was relatively good, with R^2 = 0.54 ($p < .01$), this is probably due to extensive dust emissions over LHG region, where is close to arid and semi-arid desert region in northern China.

Similarly, correlation analysis for the simulated BC and dust, BC and OC concentrations in atmospheric aerosol over the study area has been performed. Results show that there exist strong correlation between the modeled BC and OC concentrations (R^2 = 0.93) at Mt. Yulong (Fig. 11b), significantly consistent with the result found for the measured BC and OC concentrations in surface aged-snow as shown in Fig. 3. Moreover, correlation between modeled atmospheric BC and dust concentrations at ZD, XDKMD, and LHG glaciers has also been found (Fig. 11c, e, g). Similarly, results show correlation between them are relatively weak, except at LHG glacier (R^2 = 0.47), which indicates that the updated WRF-Chem model can well simulate dust and other ILAI concentrations in atmospheric aerosol over glacier regions close to or surrounded by emission sources of dust, such as arid or semi-arid region. Previous study reported that dust deposited on glaciers has complex sources, for example, local rock weathering is an important process for mineral dust particles in snow of Baishui glacier (Niu et al., 2014b). The coarse spatial resolution used in the model might also be inherently underestimating these local emission sources. Therefore, observation-constrained modeling is needed in future studies to reduce model biases and/or uncertainties in simulating ILAI concentrations in surface snow of glaciers on the TP.

CALIPSO measurements indicate that there exists a large amount of tropospheric aerosol over the west, south and north of the TP. In the western TP, there is a striking aerosol layer with altitude ranges from 0.5 to 6.0 km (Fig. 12a, b). Strong aerosol or dust signals are detected

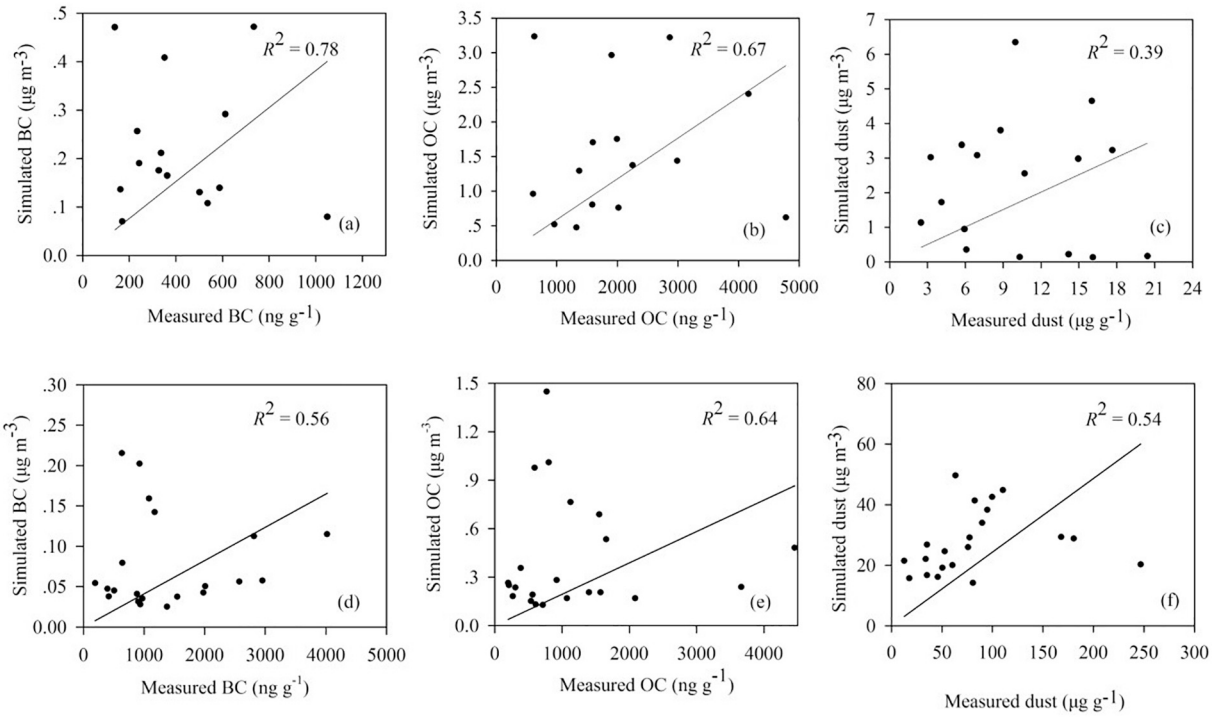

Fig. 10. Regression analysis of measured and simulated BC, OC, dust concentrations in the surface layer of snowpack and in the aerosol at surface over the Mt. Yulong (upper panel) and Laohugou glacier (Lower panel).

over Afghanistan, Pakistan, the north Arabian Sea, the west coast of India, Bay of Bengal, and the northern TP. Moreover, tropospheric aerosol vertically extended up to 8 km over the Asian Summer Monsoon region (Fig. 12). Thus atmospheric aerosols are ubiquitously distributed over the TP. The mean depolarization ratio of aerosol particles at wavelength of 532 nm in May–August 2015 was higher than that in 2014. Similarly, values of aerosol extinction coefficient at 1064 nm in May–August 2015 (Figs. S5b, d) were higher than those in 2014 (Figs. S5a, c). Atmospheric aerosol in the vertical troposphere was extensively distributed over the southern and western TP, and Asia. Therefore, annual difference of ILAIs in aerosol at surface over the glaciers (e.g., Figs. 9, S4) was largely in agreement with the disparity of tropospheric aerosol distribution in 2014 and 2015, as demonstrated from CALIPSO measurements (Figs. 12, S5). Previous studies proposed that atmospheric ILAIs transported by southwest monsoon, can reach to higher elevations in the troposphere and deposited on the glaciers over the TP (Qian et al., 2011; Niu et al., 2019). When ILAIs in the atmosphere absorbs solar radiation, the surface snow of glaciers contaminated by ILAIs absorbs more solar light and further heats the glacier surface. These effects strengthen the upward movement of the atmosphere and promote deep convection along the TP, whereas variations in atmospheric deep convection are the primary reason for vertical distribution of troposphere aerosol (Rajeevan et al., 2013).

4.5. Chemical composition of individual particles

SEM-EDX analysis is extensively used to observe and investigate the morphology and chemical composition of individual particles in cryoconite samples from Baishui glacier. Elemental signals and composition derived from SEM-EDX analysis for cryoconite samples are shown in Fig. S6. It is clear that there are abundant calcium and oxygen and diverse mineral elements in the cryoconite samples from Mt. Yulong. Based on extensive SEM-EDX observations and measurements, particle types and chemical composition of cryoconite particles were determined and illustrated in Table 2. Results indicated that calcium and silicon rich particles dominate over other elements. Individual particles can be categorized into five types according to their chemical composition and morphology derived from SEM-EDX analysis. They are composed of different mineral substances. Apart from particles rich in Ca, O, and Si element, Cu, C Au-rich particles are also considerably existed in the cryoconite samples. Chemical composition of cryoconite samples indicates the presence of carbonates, soot, tarball particles and other minerals in the cryoconite. It was reported that soot particle featured by the large aggregations of chain-type spherulites and clusters (Kocbach et al., 2006), they are typical particles originated from fossil fuel (e.g., petroleum, gasoline, diesel) and coal combustion (Frank and Herbarth, 2002). Elements of Si, Au, Cu, and Al are mostly existed in mineral substance (with irregular shapes and natural sources: soil dust, re-suspension due to anthropogenic engineering construction and transportation) in the forms of clay and feldspar particles (Cuadros et al., 2015).

Based on extensive morphological analysis, the morphology of individual particles in cryoconite samples is identified using SEM imaging method. Morphological characteristics can be used to distinguish different types of particles. Mineral particles usually have sharp edges. If the mineral particles have been transported over a long range of distances, the particles' morphology might present a round like shape. Biological particles usually have a similar morphology with fly ash particles. However, the morphology of biological particles is symmetrical, and tissue-like shape, this particular feature/trait can allow us to effectively differentiate spherical biological particles and fly ash particles. Results from the SEM-EDX analysis demonstrate that biological particles, quartz particles, fly ash particles and other aggregated-mineral particles in the cryoconite of glacier were mainly identified (Fig. 13), these types of particles are the predominant substances in the cryoconite. Actually, most of the individual particles were external or internal mixed with other kinds of particles, only a few particles were presented as single particle in the cryoconite (Dong et al., 2017). It was reported that different coating or mixing status and various morphologies greatly affect the absorption of BC-in-snow (e.g., Adachi et al.,

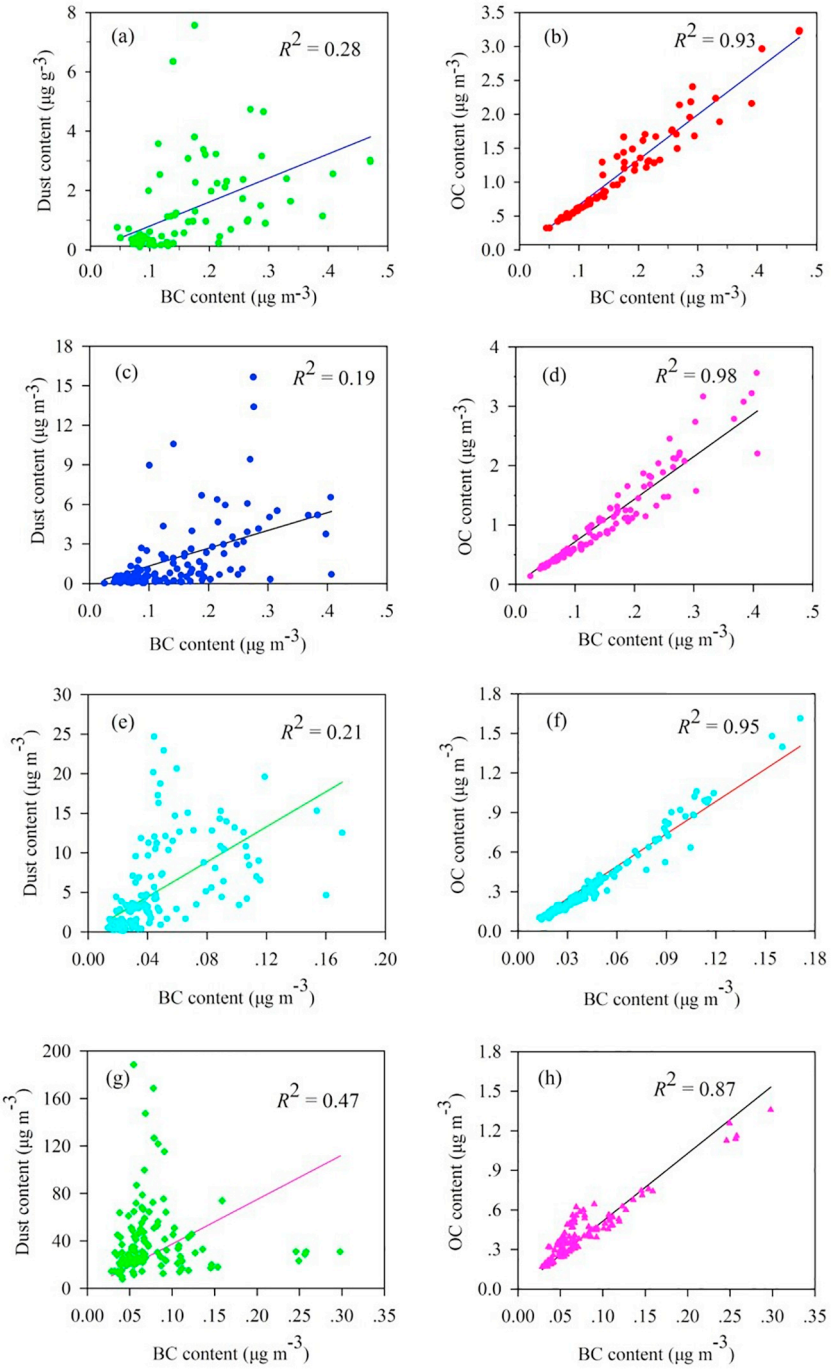

Fig. 11. Correlations between simulated near-surface atmospheric BC and dust, BC and OC concentrations at Mt. Yulong glacier (a), (b); Zhadang glacier (c), (d); DKMD glacier (e), (f); LHG glacier (g), (h).

2016). Analysis of the elemental composition using SEM imaging method provides accessional information for identification and classification of possible sources of various shapes of particles (Zhang et al., 2011). The portions of elemental composition, particle characteristics, mixing properties, and sources of different particle types are summarized in Table 3. Based on their elemental composition and morphology, the detected particles can be categorized into four types: biological particles, fly ash, soot particles, and mineral particles. This classification can facilitate us for better understanding of physiochemical properties and climatic effects of individual particles in the cryoconite of glaciers (Adachi et al., 2010; Cong et al., 2018; Lau et al., 2006; Posfai and Buseck, 2010).

5. Conclusions

To obtain a comprehensive understanding of the physicochemical process of ILAIs in snowpack and the performance of current-generation 3-D atmospheric chemical models in simulating the deposition of ILAIs in surface snow, in this study, for the first time, we systematically conducted the integrated analysis of measured and modeled concentrations of ILAI in snowpack and atmosphere at surface over the four glaciers on the TP. CALIPSO measurements were applied to investigate tropospheric aerosol and its inter-annual difference over the TP and surrounding areas. In addition, SEM-EDX analysis was employed to detect the elemental composition and morphology of particles in glacial cryoconite samples. The following conclusions can be drawn:

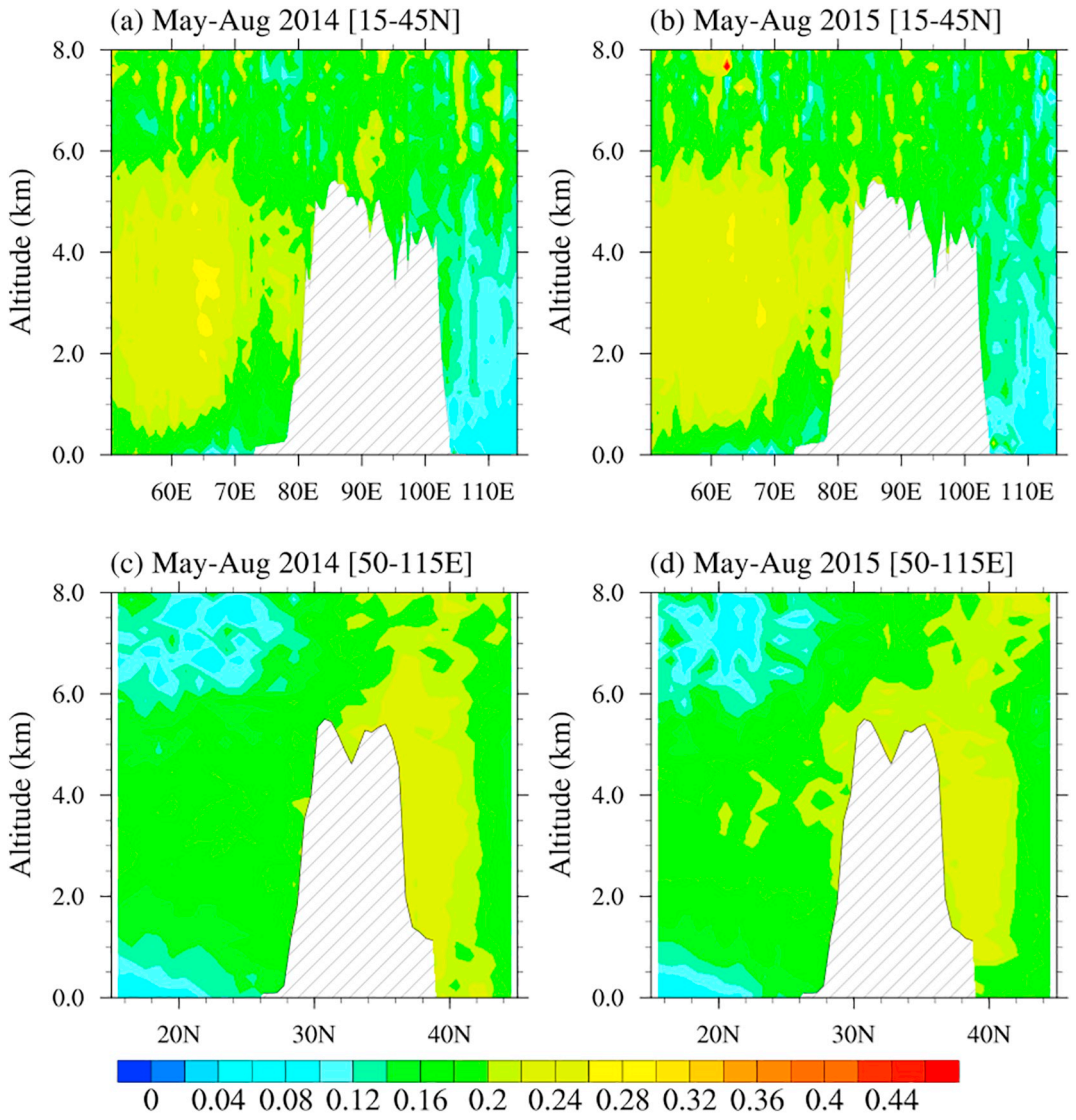

Fig. 12. Longitude-altitude cross sections and latitude-altitude cross sections of particulate depolarization ratio at wavelength of 532 nm from CALIPSO measurements in May–August 2014 (a, c) and 2015 (b, d). The latitude and longitude bounds for the average are from 15° N to 45° N and from 50° E to 115° E, respectively. The shaded parts in each plot indicate the topography of Tibetan Plateau at 30° N (a, b) and 87.5° E (c, d).

Table 2
SEM-EDX particle type and their chemical composition of individual particles in glacier cryoconite on Mt. Yulong.

Type	Ratio (%)	Mass percentage of various chemical elements (%)										
		Ca	Au	Cu	C	Si	Al	Fe	K	Mg	Zn	N
Ca-rich	45.4	45.2	6.6	1.2	–	**–**	–	–	–	0.2	–	–
Si, Cu-rich	31.36	**–**	10.8	**12.8**	6.2	**18.4**	4.98	3.98	1.07	1.43	7.61	–
Si, Au-rich	33.23	**–**	**12**	–	**–**	**20.9**	9.63	7.73	5.1	**–**	–	9.3
Si, C, Au-rich	46.1	0.9	**12.1**	**–**	**14.4**	**19.6**	8.94	7.36	2.92	1.21	–	–
Ca, C-rich	52.9	**41.2**	**–**	1.2	**8.5**	1.5	0.82	0.64	–	–	–	–

Bold indicates the mean difference is significant at the 0.05 level.

(1) Strong correlation between BC and dust has been found in surface aged-snow samples, while the correlation significantly varied with the depth of snowpit. Evolution of the correlation between BC and dust concentrations in snowpack indirectly emphasizes the significance of inherent physiochemical and post-depositional processes inside snowpacks.
(2) BC and OC concentrations in snowpits tended to decrease with depth. The ratio of OC to BC was between 2 and 3 except a higher value found at depth bin of 1.5–2.0 m. In contrast, average dust concentrations in the vertical snowpit were similar at 0.0–2.0 m from the surface. Mean OC concentrations were consecutively decreased from the top to the bottom of snowpits. Significant differences of BC and OC, and dust concentrations among depth intervals/bins reflect their different hydrophilicities, physiochemical properties and post-depositional processes in snowpit, offering important observational constraints on the related processes.
(3) Optical properties ATN of BC gradually decreased vertically with depth in snowpit. Surface aged-snow has the highest ATN value

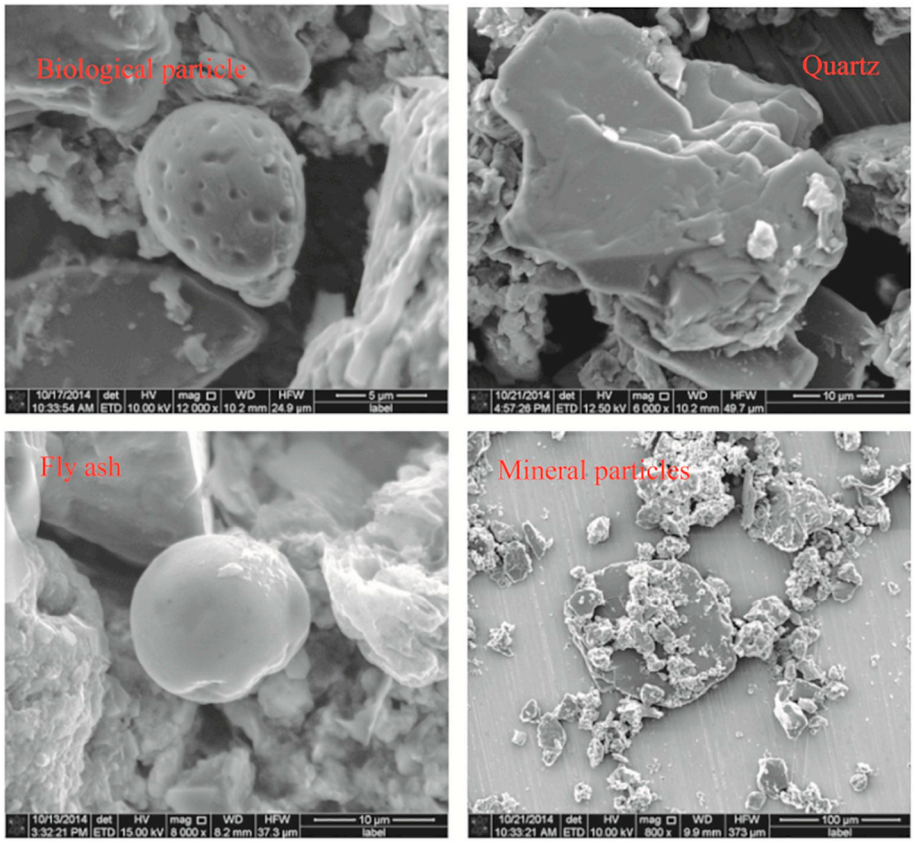

Fig. 13. Typical morphology of individual particles in the glacier cryoconite from Mt. Yulong detected using scanning electron microscopy, coupled with energy dispersive X-ray spectrometer (SEM-EDX) method.

(0.25 ± 0.012), snow samples from the bottom of snowpit (2.0–2.5 m) had the lowest ATN value (0.11 ± 0.018). In contrast, BC MAC significantly increased with depth increment from the surface to the bottom of snowpit. Snow samples of 2.0–2.5 depth interval had the highest BC MAC value (8.51 ± 1.05 $m^2\ g^{-1}$). The larger change of BC MAC than ATN with depth in snowpit reflects the physical and chemical processing of BC in snowpack.

(4) Observation data showed that from May to August, monthly variation of the modeled ILAI concentrations significantly decreased. The monthly trend of ILAIs is characterized by distinct spatial heterogeneity. LHG glacier has the highest impurity concentration among the four investigated glaciers on the TP, followed by high BC and OC contents in snow of Yulong glacier. ILAI concentrations in surface snow in May–August 2015 were apparently higher than those in 2014. CALIPSO measurements showed a striking aerosol layer with altitude from 0.5 to 6.0 km. Tropospheric aerosol vertically extended up to 8 km over the Asian Summer Monsoon region. The annual difference of ILAIs in surface snow of glaciers was in qualitative agreement with the difference of tropospheric aerosol distribution in 2014 and 2015. However, further in-depth field observations are quite necessary to improve future simulations of ILAIs in snow of glaciers on the TP.

(5) SEM-EDX observations and measurements indicated calcium and silicon rich particles dominated over other elements. Cu, C, Au-rich particles were also noticeably in the cryoconite samples. Biological particles, quartz particles, fly ash particles and other aggregated-mineral particles in the glacier cryoconite were also found. These four types of particles were the predominant substances in the cryoconite. The classification and SEM-EDX analysis can facilitate better understanding of the physicochemical properties and climatic effects of particles in the glacial cryoconite.

(6) The quasi-global channel WRF-Chem model can well simulate atmospheric dust and other ILAI concentrations over glacier regions where are close to or are surrounded by emission sources of dust. A few factors can be used to explain the differences between measured and grid-simulated concentrations of ILAI. Thus observation-constrained modeling is needed for the future studies to improve model formulation/performance and reduce model uncertainties of the simulated ILAI concentrations in snowpack.

Data availability

Our underlying research data was obtained from much field work and laboratory analysis and model simulation, the data used in this study are original and can be obtained from the corresponding author.

Declarations of Competing Interest

None.

Author contributions

All authors designed the research framework. H. Niu contributed to field work, laboratory analysis and paper writing. S. Kang and Y. Wang contributed to manuscript organization and guidance. S. Chandan and Y. Qian performed model simulations, D. Rupakheti proposed some useful suggestions.

Acknowledgments

This work was supported by the National Natural Science Foundation of China (41971080, 41721091), the second Tibetan Plateau Scientific Expedition and Research Program (STEP) (2019QZKK0605), the independent program of SKLCS (SKLCS-ZZ-

Table 3
Classification criteria of the identified particle types, mixing properties and the potential sources.

Particle types	Element composition	Mixing states	Potential sources	References
Biological particles	K, S, Fe, Mg, Ca, C, and other oxides	Internal or external mixed with other particles, organic substance	Pollen, spores, algae, fungi, fragments of insect and leaves, the excrements of insect	Wittmaack et al., 2005; Cong et al., 2010.
Fly ash	Si, Al, Fe, and S-rich	Fly ash mixed with salt (nitrate, sulfate), metal oxide, silicate containing minor Fe, Mn and other metals	Thermal power plant, heavy industries, and oil refinery	Shi et al., 2003; Li et al., 2014; Zhang et al., 2011
Soot particles	C-dominant, O-rich	C-rich materials mixed with organic, S, and K-rich articles.	Biomass burning, fossil fuels combustion	Dong et al., 2017; Li et al., 2014; Goldstein, 2003
Mineral particles	Si, Ca, Al, Mg, Fe-rich, e.g., quartz, clay, feldspar, albite, and other oxides.	Minerals aggregated and mixed with soot and salt	Crustal dust, surface soil, desert sand, etc.	Li and Shao, 2009; Laskin et al., 2005; Dong et al., 2015.

2020). We also thank the support of the Key Research Program for Frontier Sciences of Chinese Academy of Sciences (QYZDJ-SSW-DQC039). The Pacific Northwest National Laboratory (PNNL) is operated for DOE by Battelle Memorial Institute under contract DE-AC05-76RLO1830. The CALIPSO data used in this study was obtained from the NASA Langley Research Center Atmospheric Science Data Center.

Competing interests

The authors of this manuscript declare that they have no conflict of interest.

Appendix A. Supplementary data

Supplementary data to this article can be found online at https://doi.org/10.1016/j.atmosres.2020.105002.

References

Aamaas, B., Bøggild, C.E., Stordal, F., 2011. Elemental carbon deposition to Svalbard snow from Norwegian settlements and long-range transport. Tellus B 63, 340–351. https://doi.org/10.1111/j.1600-0889.2011.00531.x.

Adachi, K., Chung, S.H., Buseck, P.R., 2010. Shapes of soot aerosol particles and implications for their effects on climate. J. Geophys. Res. 115, D15206. https://doi.org/10.1029/20. 09JD012868.

Adachi, K., Moteki, N., Kondo, Y., Igrashi, Y., 2016. Mixing states of light-absorbing particles measured using a transmission electron microscope and a single-particle soot photometer in Tokyo, Japan. J. Geophys. Res. 12, 9153–9164. https://doi.org/10.1002/2016JD025153.

Anderson, C.H., Dibb, J.E., Griffin, R.J., Hagler, G.S.W., Bergin, M.H., 2008. Atmospheric water-soluble organic carbon measurements at Summit, Greenland. Atmos. Environ. 42, 5612–5621. https://doi.org/10.1016/j.atmosenv.2008.03.006.

Aoki, T., Aoki, T., Fukabori, M., Uchiyama, A., 1999. Numerical simulation of the atmospheric effects on snow albedo with a multiple scattering radiative transfer model for the atmosphere-snow system. J. Meteor. Soc. Japan 77 (2), 595–614.

Bergin, M.H., Ghoroi, C., Dixit, D., Schauer, J.J., Shindell, D.T., 2017. Large reductions in solar energy production due to dust and particulate air pollution. Environ. Sci. Technol. Lett. 4 (8), 339–344. https://doi.org/10.1021/acs.estlett.7b00197.

Bond, T.C., Habib, G., Bergstrom, R.W., 2006. Limitations in the enhancement of visible light absorption due to mixing state. J. Geophys. Res. 111, D20211. https://doi.org/10.1029/2006JD007315.

Bond, T.C., Doherty, S.J., Fahey, D.W., Forster, P.M., Berntsen, T., DeAngelo, B.J., Flanner, M.G., Ghan, S., Karcher, B., Koch, D., Kinne, S., Kondo, Y., Quinn, P.K., Sarofim, M.C., Schultz, M.G., Schulz, M., Venkataraman, C.V., Zhang, H., Zhang, S., Bellouin, N., Guttikunda, S.K., Hopke, P.K., Jacobson, M.Z., Kaiser, J.W., Klimont, Z., Lohmann, U., Schwarz, J.P., Shindell, D., Storelvmo, T., Warren, S.G., Zender, C.S., 2013. Bounding the role of black carbon in the climate system: A scientific assessment. J. Geophys. Res.-Atmos. 118, 5380–5552. https://doi.org/10.1002/jgrd.50171.

Cappa, C.D., et al., 2012. Radiative absorption enhancements due to the mixing state of atmospheric black carbon. Science 31 (337), 1078–1081.

Cheng, Y., He, K.B., Zheng, M., Duan, F.K., Du, Z.Y., Ma, Y.L., Tan, J.H., 2011. Mass absorption efficiency of elemental carbon and water-soluble organic carbon in Beijing, China. Atmos. Chem. Phys. 11, 11497–11510. https://doi.org/10.5194/acpd-11-6221-2011.

Cong, Z.Y., Kang, S.C., Dong, S.P., Liu, X.D., Qin, D.H., 2010. Elemental and individual particle analysis of atmospheric aerosols from high Himalayas. Environ. Monit. Assess. 160, 323–335 http://link.springer.com/article/10.1007%2Fs10661-008-0698-3.

Cong, Z., et al., 2018. Iron oxides in the cryoconite of glaciers on the Tibetan plateau: abundance, speciation and implications. The Cryosphere 12 (10), 3177–3186. https://doi.org/10.1016/s1001-0742(09)60269-2.

Conway, H., Gades, A., Raymond, C.F., 1996. Albedo of dirty snow during conditions of melt. Water Resour. Res. 32 (6), 1713–1718. https://doi.org/10.1029/96WR00712.

Cuadros, J., Diaz-Hernandez, J.L., Sanchez-Navas, A., Garcia-Casco, A., 2015. Role of clay minerals in the formation of atmospheric aggregates of Saharan dust. Atmos. Environ. 120, 160–172. https://doi.org/10.1016/j.atmosenv.2015.08.077.

Dang, C., Fu, Q., Warren, S.G., 2016. Effect of snow grain shape on snow albedo. J. Atmos. Sci. 73, 3573–3583. https://doi.org/10.1175/JAS-D-15-0276.1.

Doherty, S.J., Warren, S.G., Grenfell, T.C., Clarke, A.D., Brandt, R.E., 2010. Light-absorbing impurities in Arctic snow. Atmos. Chem. Phys. 10, 11647–11680. https://doi.org/10.5194/acp-10-11647-2010.

Doherty, S.J., Grenfell, T.C., Forsström, S., Hegg, D.L., Brandt, R.E., Warren, S.G., 2013. Observed vertical redistribution of black carbon and other insoluble light-absorbing particles in melting snow. J. Geophys. Res. Atmos. 118. https://doi.org/10.1002/jgrd.50235.

Dong, Z.W., Kang, S.C., Qin, X., 2015. New insights into trace elements deposition in the snow packs at remote alpine glaciers in the northern Tibetan Plateau, China. Sci. Total Environ. 529, 101–113. https://doi.org/10.1016/j.scitotenv.2015.05.065.

Dong, Z.W., Kang, S.C., Guo, J.M., Zhang, Q.Q., Wang, X.J., Qin, D.H., 2017. Composition

and mixing states of brown haze particle over Himalayas along two transboundary south-north transects. Atmos. Environ. 156, 24–35. https://doi.org/10.1016/j.atmosenv.2017.02.029.
Flanner, M.G., Zender, C.S., 2006. Linking snowpack microphysics and albedo evolution. J. Geophys. Res.-Atmos. 111, D12208. https://doi.org/10.1029/2005jd006834.
Flanner, M.G., Zender, C.S., Randerson, J.T., Rasch, P.J., 2007. Present-day climate forcing and response from black carbon in snow. J. Geophys. Res. 112, D11202. https://doi.org/10.1029/2006JD008003.
Gertler, C.G., Puppala, S.P., Panday, A., Stumm, D., Shea, J., 2016. Black carbon and the Himalayan cryosphere: a review. Atmos. Environ. 125, 404–417. https://doi.org/10.1016/j.atmosenv.2015.08.078.
Ginoux, P., Chin, M., Tegen, I., Prospero, J.M., Holben, B., Dubovik, O., Lin, S.J., 2001. Sources and distributions of dust aerosols simulated with the GOCART model. J. Geophys. Res. 106, 20255–20273. https://doi.org/10.1029/2000JD000053.
Goldstein, J., 2003. Scanning electron microscopy and X-ray microanalysis. Kluwer, New York, pp. 1–223. https://doi.org/10.1007/978-1-4613-0491-3_5.
Guenther, A., Zimmerman, P., Wildermuth, M., 1994. Natural volatile organic compound emission rate estimates for US woodland landscapes. Atmos. Environ. 28, 1197–1210 doi:10.1016/1352- 2310(94)90297-6.
Hadley, O.L., Kirchstetter, T.W., 2012. Black-carbon reduction of snow albedo. Nat. Clim. Change 437–440. https://doi.org/10.1038/NCLIMATE1433.
Hu, Z., Zhao, C., Huang, J., Leung, L.R., Qian, Y., Yu, H., Huang, L., Kalashnikova, O.V., 2016. Trans-Pacific transport and evolution of aerosols: evaluation of quasi-global WRF-Chem simulation with multiple observations. Geosci. Model Dev. 9, 1725–1746. https://doi.org/10.5194/gmd-2015-248.
Immerzeel, W., VanBeek, L.P.H., Bierkens, M.F.P., 2010. Climate change will affect the Asian water towers. Science 328, 1382–1385. https://doi.org/10.1126/science.1183188.
IPCC, 2013. Summary for Policymakers. In: Stocker, T.F., Qin, D., Plattner, G.-K., Tignor, M., Allen, S.K., Boschung, J. ... Midgley, P.M. (Eds.), Climate Change 2013: The Physical Science Basis. Contribution of Working Group I to the Fifth Assessment Report of the Intergovernmental Panel on Climate Change. Cambridge University Press, Cambridge, United Kingdom and New York, NY, USA.
Jacobi, H.W., Lim, S., Ménégoz, M., Ginot, P., Laj, P., Bonasoni, P., Stocchi, P., Marinoni, A., Arnaud, Y., 2015. Black carbon in snow in the upper Himalayan Khumbu Valley, Nepal: observations and modeling of the impact on snow albedo, melting, and radiative forcing. Cryosphere 9, 1685–1699.
Jacobson, M.Z., 2001. Strong radiative heating due to the mixing state of black carbon in atmospheric aerosols. Nature 409, 695–697. https://doi.org/10.1038/35055518.
Jacobson, M.Z., 2005. A refined method of parameterizing absorption coefficients among multiple gases simultaneously from line-by-line data. J. Atmos. Sci. 62, 506–517. https://doi.org/10.1175/JAS-3372.1.
Ji, Z., 2016. Modeling black carbon and its potential radiative effects over the Tibetan Plateau. Adv. Clim. Change Res. 7, 139–144 doi:CNKI:SUN:QHYJ.0.2016–03-005.
Kang, S., Zhang, Q., Qian, Y., Ji, Z., Li, C., Cong, Z., Zhang, Y., Guo, J., Du, W., Huang, J., You, Q., Panday, A.K., Rupakheti, M., Chen, D., Gustafsson, Örjan, Thiemens, M.H., Qin, D., 2019. Linking atmospheric pollution to cryospheric change in the Third Pole Region: current progresses and future prospects. Natl. Sci. Rev. https://doi.org/10.1093/nsr/nwz031. nwz031.
Kaspari, S.D., Painter, T.H., Gysel, M., et al., 2014. Seasonal and elevational variations of black carbon and dust in snow and ice in the Solu-Khumbu, Nepal and estimated radiative forcings. Atmos. Chem. Phys. 14, 8089–8103. https://doi.org/10.5194/acp-14-8089-2014.
Kaspari, S., Skiles, S.M., Delaney, I., Dixon, D., Painter, T.H., 2015. Accelerated glacier melt on Snow Dome, Mount Olympus, Washington, USA, due to deposition of black carbon and mineral dust from wild fire. J. Geophys. Res. Atmos 120, 2793–2807. https://doi.org/10.1002/2014JD022676.
Knox, A., Evans, G.J., Brook, J.R., Yao, X., Jeong, C.H., Godri, K.J., Sabaliauskas, K., Slowik, J.G., 2009. Mass absorption cross-section of ambient black carbon aerosol in relation to chemical age. Aerosol Sci. Technol. 43, 522–532. https://doi.org/10.1080/02786820902777207.
Kocbach, A., Li, Y., Yttri, K.E., et al., 2006. Physicochemical characterization of combustion particles from vehicle exhaust and residential wood smoke. Part. Fibre Toxicol. 3 (1), 1–10. https://doi.org/10.1186/1743-8977-3-1.
Laskin, A., Iedema, M.J., Ichkovich, A., 2005. Direct observation of completely processed calcium carbonate dust particles. Faraday Discuss. 130, 453–468. https://doi.org/10.1039/B417366J.
Lau, K.M., Kim, M.K., Kim, K.M., 2006. Asian summer monsoon anomalies induced by aerosol direct forcing: the role of the Tibetan Plateau. Clim. Dynam. 26, 855–864 doi:10.10 07/s0 0382–0 06–0114-z.
Lau, K.M., Kim, M.K., Kim, K.M., Lee, W.S., 2010. Enhanced surface warming and accelerated snow melt in the Himalayas and Tibetan Plateau induced by absorbing aerosols. Environ. Res. Let. 5, 025204. https://doi.org/10.1088/1748-9326/5/2/025204.
Lau, W.K.M., Sang, J., Kim, M.K., Kim, K.M., Koster, R.D., Yasunari, T.J., 2018. Effects of snow darkening by deposition of light-absorbing aerosols on hydroclimate of Eurasia during boreal spring and summer. J. Geophys. Res. 631, 8441–8461. https://core.ac.uk/display/10512951.
Lee, W.S., Kim, M.K., 2010. Effects of radiative forcing by black carbon aerosol on spring rainfall decrease over Southern Asia. Atmos. Environ. 44, 3739–3744. https://doi.org/10.1016/j.atmosenv.2010.06.058.
Lee, Y.H., et al., 2013. Evaluation of preindustrial to present-day black carbon and its albedo forcing from Atmospheric Chemistry and Climate Model Intercomparison Project (ACCMIP). Atmos. Chem. Phys. 13, 2607–2634. https://doi.org/10.5194/acp-13-2607-2013.
Li, W.J., Shao, L.Y., 2009. Observation of nitrate coatings on atmospheric mineral dust particles. Atmos. Chem. Phys. 9 (6), 1863–1871. www.atmos-chem-phy.net/9/1863/2009.
Li, W.J., Shao, L., Shi, Z., 2014. Mixing state and hygroscopicity of dust and haze particles before leaving Asian continent. J. Geophys. Res. Atmos. 119, 1044–1059. https://doi.org/10.1002/2013JD021003.
Li, Z.X., Feng, Q., Guo, X.Y., Gao, Y., Pan, Y.H., Wang, T.T., Li, J.G., Guo, R., Jia, B., Song, Y.X., 2015. The evolution and environmental significance of glaciochemistry during the ablation period in the north of Tibetan Plateau, China. Quatern. Int. 374, 93–109. https://doi.org/10.1016/j.quaint.2014.06.071.
Li, Z.X., Feng, Q., Wang, Q.J., Yong, S., Li, J.G., Li, Y.G., 2016. The influence from the shrinking cryosphere and strengthening evopotranspiration on hydrologic process in a cold basin, Qilian Mountains. Glob. Planet. Chang. 144, 119–128. https://doi.org/10.1016/j.gloplacha.2016.06.017.
Li, X.F., Kang, S.C., He, X.B., Qu, B., Tripathee, L., Jing, Z., Paudyal, R., Li, Y., Zhang, Y., Yan, F., Li, G., Li, C.L., 2017. Light-absorbing impurities accelerate glacier melt in the Central Tibetan Plateau. Sci. Total Environ. 587–588, 482–490. https://doi.org/10.1016/j.scitotenv.2017.02.169.
Li, X.F., Kang, S.C., Zhang, G.S., Qu, B., Tripathee, L., 2018. Light-absorbing impurities in a southern Tibetan Plateau glacier: Variations and potential impact on snow albedo and radiative forcing. Atmos. Res. 200, 77–87.
Li, Y., Kang, S.C., Chen, J.Z., Hu, Z.F., Wang, K., Paudyal, R., et al., 2019. Black carbon in a glacier and snow cover on the northeastern Tibetan Plateau: Concentrations, radiative forcing and potential source from local topsoil. Sci. Total Environ. 686, 1030–1038. https://doi.org/10.1016/j.scitotenv.2019.05.469.
Lim, S., Faïn, X., Zanatta, M., Cozic, J., Jaffrezo, J.L., Ginot, P., Laj, P., 2014. Refractory black carbon mass concentrations in snow and ice: Method evaluation and intercomparison with elemental carbon measurement. Atmospheric Measurement Techniques 7, 3307–3324.
Liou, K.N., Takano, Y., He, C., Yang, P., Leung, L.R., Gu, Y., Lee, W.L., 2014. Stochastic parameterization for light absorption by internally mixed BC/dust in snow grains for application to climate models. J. Geophys. Res. Atmos. 119, 7616–7632. https://doi.org/10.1002/2014JD021665.
Liu, J.B., Rühland, K.M., Chen, J.H., Xu, Y.Y., Chen, S.Q., Chen, Q.M., Huang, W., Xu, Q.H., Chen, F.H., Smol, J.P., 2017. Aerosol-weakened summer monsoons decrease lake fertilization on the Chinese Loess Plateau. Nat. Clim. Chang. 7, 190–194. https://doi.org/10.1038/NCLIMATE3220.
Ming, J., Wang, P.L., Zhao, S.Y., Chen, P.F., 2013. Disturbance of light-absorbing aerosols on the albedo in a winter snowpack of Central Tibet. J. Environ. Sci. 25 (8), 1601–1607. https://doi.org/10.1016/S1001-0742(12)60220-4.
Molot, L.A., Dillon, P.J., 1997. Photolytic regulation of dissolved organic carbon in northern lakes. Global Biochem. Cy. 11, 351–365. https://doi.org/10.1029/97gb01198.
Niu, H.W., He, Y.Q., Lu, X.X., Shen, J., Du, J.K., Zhang, T., Pu, T., 2014. Chemical composition of rainwater in the Yulong Snow Mountain region, Southwestern China. Atmos. Res. 144, 195–206. https://doi.org/10.1016/j.atmosres.2014.03.010.
Niu, H.W., He, Y.Q., Lu, X.X., Dong, Z.W., 2014b. Characteristics of modern atmospheric dust deposition in snow in the Mt. Yulong region, southeastern Tibetan Plateau. J. Asian Earth Sci. 94, 45–54. https://doi.org/10.1016/j.jseaes.2014.08.003.
Niu, H.W., He, Y.Q., Kang, S.C., 2016. Chemical compositions of snow from Mt. Yulong, southeastern Tibetan Plateau. J. Earth Syst. Sci. 125 (2), 403–416. https://doi.org/10.1007/s12040-016-0670-5.
Niu, H.W., Kang, S.C., Shi, X.F., 2017a. In-situ measurements of light-absorbing impurities in snow of glacier on Mt. Yulong and implications for radiative forcing estimates. Sci. Tot. Environ. 581–582, 848–856. https://doi.org/10.1016/j.scitotenv.2017.01.032.
Niu, H.W., Kang, S.C., Zhang, Y.L., Shi, X.F., 2017b. Distribution of light-absorbing impurities in snow of glacier on Mt. Yulong, southeastern Tibetan Plateau. Atmos. Res. 197, 474–484. https://doi.org/10.1016/j.atmosres.2017.07.004.
Niu, H.W., Kang, S.C., Wang, H.L., Zhang, R.D., et al., 2018. Seasonal variation and light absorption property of carbonaceous aerosol in a typical glacier region of the southeastern Tibetan Plateau. Atmos. Chem. Phys. 18, 6441–6460. https://doi.org/10.5194/acp-18-6441-2018.
Niu, H.W., Kang, S.C., Gao, W.N., Wang, Y.H., 2019. Vertical distribution of the Asian tropopause aerosols detected by CALIPSO. Environ. Pollut. 253, 207–220. https://doi.org/10.1016/j.envpol.2019.06.111.
Nordmann, S., Birmili, W., Weinhold, K., Müller, K., Spindler, G., Wiedensohler, A., 2013. Measurements of the mass absorption cross section of atmospheric soot particles using Raman spectroscopy. J. Geophys. Res. Atmos. 118https://doi.org/10.1002/2013JD020021. 12, 075-12, 085.
Posfai, M., Buseck, P.R., 2010. Nature and climate effects of individual tropospheric aerosol particles. Annu. Rev. Earth Planet. Sci. 38 (1), 17–43. https://doi.org/10.1146/annurev.earth.031208.100032.
Qian, Y., Flanner, M.G., Leung, L.R., Wang, W., 2011. Sensitivity studies on the impacts of Tibetan Plateau snowpack pollution on the Asian hydrological cycle and monsoon climate. Atmos. Chem. Phys. 11 (1929–727), 1948. https://doi.org/10.5194/acp-11-1929-2011.
Qian, Y., Yasunari, T.J., Doherty, S.J., Flanner, M.G., Lau, W.K.M., Ming, J., Wang, H., Wang, M., Warren, S.G., Zhang, R., 2015. Light-absorbing particles in snow and ice: measurement and modeling of climatic and hydrological impact. Adv. Atmos. Sci. 32, 64–91. https://doi.org/10.1007/s00376-014-0010-0.
Rajeevan, M., Rohini, P., Niranjan Kumar, K., Srinivasan, J., Unnikrishnan, C.K., 2013. A study of vertical cloud structure of the Indian summer monsoon using CloudSat data. Clim. Dyn. 40, 637e650. https://doi.org/10.1007/s00382-012-1374-4.
Ramanathan, V., Carmichael, G., 2008. Global and regional climate changes due to black carbon. Nat. Geosci. 1, 221–227. https://doi.org/10.1038/ngeo156.
Sarangi, C., Qian, Y., Rittger, K., Bormann, K.J., Liu, Y., Wang, H., Wan, H., Lin, G.,

Painter, T.H., 2019. Impact of light-absorbing particles on snow albedo darkening and associated radiative forcing over high-mountain Asia: high-resolution WRF-Chem modeling and new satellite observations. Atmos. Chem. Phys. 19, 7105–7128. https://doi.org/10.5194/acp-19-7105-2019.

Schnaiter, M., Linke, C., Mohler, O., Naumann, K.H., Saathoff, H., Wagner, R., Schurath, U., Wehner, B., 2005. Absorption amplification of black carbon internally mixed with secondary organic aerosol. J. Geophys. Res. 110, D19204. https://doi.org/10.1029/2005JD006046.

Schuckmann, K.V., Palmer, M.D., Trenberth, K.E., 2016. An imperative to monitor Earth's energy imbalance. Nat. Clim. Change 6. https://doi.org/10.1038/NCLIMATE2876.

Schultz, M., Rast, S., van het Bolscher, M., Pulles, T., Brand, R., Pereira, J., Mota, B., Spessa, A., Dalsren, S., van Nojie, T., and Szopa, S.: Emission data sets and methodologies for estimating emissions, RETRO project report D1–6, Hamburg, available at: http://retro-archive.iek.fz-juelich.de/data/documents/reports/ D1-6_final.pdf (last access: 3 May 2016), 2007.

Shi, Z.B., Shao, L.Y., Jones, T.P., 2003. Characterization of airborne individual particles collected in an urban area, a satellite city and a clean air area in Beijing, 2001. Atmos. Environ. 37 (29), 4097–4108. https://doi.org/10.1016/S1352-2310(03)00531-4.

Si, M., Irish, V.E., Mason, R.H., Vergara-Temprado, J., Hanna, S.J., Ladino, L.A., Yakobi-Hancock, J.D., Schiller, C.L., Wentzell, J.J.B., Abbatt, J.P.D., Carslaw, K.S., Murray, B.J., Bertram, A.K., 2018. Ice-nucleating ability of aerosol particles and possible sources at three coastal marine sites. Atmos. Chem. Phys. 18, 15669–15685. https://doi.org/10.5194/acp-18-15669-2018.

Skeie, R.B., Berntsen, T., Myhre, G., 2011. Black carbon in the atmosphere and snow, from preindustrial times until present. Atmos. Chem. Phys. 11, 6809–6836. https://doi.org/10.5194/acp-11-6809-2011.

Skiles, M., Painter, T.H., 2018. Assessment of radiative forcing by light-absorbing particles in snow from in situ observations with radiative transfer modeling. J. Hydrometeorol. 19, 1397–1409.

Tegen, I., Werner, M., Harrison, S.P., Kohfeld, K.E., 2004. Relative importance of climate and land use in determining present and future global soil dust emission. Geophys. Res. Lett 31, L05105 10.1029/20 03GL019216.

Tranter, M., Tsiouris, S., Davies, T.D., Jones, H.G., 1992. A laboratory investigation of the leaching of solute from snowpack by rainfall. Hydrol. Process. 6 (2), 169–178. https://doi.org/10.1002/hyp.3360060205.

Wang, P., Li, Z., Gao, W., 2011. Rapid shrinking of glaciers in the middle Qilian Mounta region of Northwest China during the last ~50 years. J. Earth Sci. 22 (4), 539–554. https://doi.org/10.1007/s12583-011-0195-4.

Wang, M., Xu, B.Q., Cao, J.J., 2015. Carbonaceous aerosols recorded in a southeastern Tibetan glacier: analysis of temporal variations and model estimates of sources and radiative forcing. Atmos. Chem. Phys. 15, 1191–1204. https://doi.org/10.5194/acp-15-1191-2015.

Warren, S.G., Wiscombe, W.J., 1980. A model for the spectral albedo of snow. II: Snow containing atmospheric aerosols. J. Atmos. Sci 37, 2734–2745. https://doi.org/10.1175/1520-0469(1980)037<2734:AMFTSA>2.0.CO;2.

Wipf, S., Sommerkorn, M., Stutter, M.I., Wubs, E.R.J., Wal, R., 2015. Snow cover, freeze-thaw, and the retention of nutrients in an oceanic mountain ecosystem. Ecosphere. 6 (10), 207. https://doi.org/10.1890/ES15-00099.1.

Wittmaack, K., Wehnes, H., Heinzmann, U., Agerer, R., 2005. An overview on bioaerosols viewed by scanning electron microscopy. Sci. Total Environ. 346 (1–3), 244–255. https://doi.org/10.1016/j.scitotenv.2004.11.009.

Xu, B.Q., Wang, M., Joswiak, D.R., et al., 2009. Deposition of anthropogenic aerosols in a southeastern Tibetan glacier. J. Geophys. Res. 114, D17209 doi:10. 1029/2008JD011510.

Xu, B.Q., Cao, J.J., Joswiak, X., et al., 2012. Post-depositional enrichment of black soot in snowpack and accelerated melting of Tibetan glaciers. Environ. Res. Lett. 7. https://doi.org/10.1088/1748-9326/7/014022.

Yang, S., Xu, B.Q., Cao, J.J., et al., 2015. Climate effect of black carbon aerosol in a Tibetan Plateau glacier. Atmos. Environ. 111, 71–78. https://doi.org/10.1016/j.atmosenv.2015.03.016.

Yao, T., Thompson, L.G., Mosbrugger, V., Zhang, F., Ma, Y., Luo, T., Xu, B., Yang, X., Joswiak, D.R., Wang, W., Joswiak, M.E., Devkota, L.P., Tayal, S., Jilani, R., Fayziev, R., 2012. Third Pole Environment (TPE). Environ. Dev. 3, 52–64. https://doi.org/10.1016/j.envdev.2012.04.002.

You, Q.L., Kang, S.C., Pepin, N., Fluegel, W.A., Yan, Y., Behrawan, H., Huang, J., 2010. Relationship between temperature trend magnitude, elevation and mean temperature in the Tibetan Plateau from homogenized surface stations and reanalysis data. Glob. Planet. Change 71, 124–133. https://doi.org/10.1016/j.gloplacha.2010.01.020.

Zaveri, R.A., Peters, L.K., 1999. A new lumped structure photochemical mechanism for large-scale applications. J. Geophys. Res. 104, 30387–30415. https://doi.org/10.1029/1999JD900876.

Zaveri, R.A., Easter, R.C., Fast, J.D., Peters, L.K., 2008. Model for Simulating Aerosol Interactions and Chemistry (MOSAIC). J. Geophys. Res. 113, D13204. https://doi.org/10.1029/2007JD008782.

Zhang, Q., Streets, D.G., Carmichael, G.R., He, K.B., Huo, H., Kannari, A., Klimont, Z., Park, I.S., Reddy, S., Fu, J.S., Chen, D., Duan, L., Lei, Y., Wang, L.T., Yao, Z.L., 2009. Asian emissions in 2006 for the NASA INTEX-B mission. Atmos. Chem. Phys. 9, 5131–5153. https://doi.org/10.5194/acp-9-5131-2009.

Zhang, X.L., Wu, G.J., Yao, T.D., et al., 2011. Characterization of individual fly ash particles in surface snow at Urumqi Glacier No. 1, Eastern Tianshan. Chinese Sci. Bull. 56, 3464–3473. https://doi.org/10.1007/s11434-011-4684-8.

Zhang, Y.L., Li, B.Y., Zheng, D., 2014. Datasets of the boundary and area of the Tibetan Plateau. Global Change Research Data Publishing and Repository 69, 164–168. https://doi.org/10.3974/geodb. 2014.01.12.v 1.

Zhang, Y.L., Kang, S.C., Li, C.L., Gao, T.G., Cong, Z.Y., Sprenger, M., et al., 2017. Characteristics of black carbon in snow from Laohugou No. 12 glacier on the northern Tibetan Plateau. Sci. Total Environ 607–608, 1237–1249.

Zhang, Y.L., Kang, S.C., Sprenger, M., Cong, Z.Y., Gao, T.G., Li, C.L., Ta, S., Li, X.F., Zhong, X.Y., Xu, M., Meng, W.J., Neupane, B., Qin, X., Sillanpää, M., 2018. Black carbon and mineral dust in snow cover on the Tibetan Plateau. Cryosphere 12, 413–431. https://doi.org/10.5194/tc-12-413-2018.

Zhao, C., Chen, S., Leung, L.R., Qian, Y., Kok, J.F., Zaveri, R.A., Huang, J., 2013a. Uncertainty in modeling dust mass balance and radiative forcing from size parameterization. Atmos. Chem. Phys. 13, 10733–10753. https://doi.org/10.5194/acp-13-10733-2013.

Zhao, C., Leung, L.R., Easter, R., Hand, J., Avise, J., 2013b. Characterization of speciated aerosol direct radiative forcing over California. J. Geophys. Res. 118, 2372–2388. https://doi.org/10.1029/2012JD018364.

Ziskin, D., 2016. MOPITT Level 3 CO Gridded Daily Means (Near and Thermal Infrared Radiances) HDF File - Version 7 [Data set]. NASA Langley Research Center Atmospheric Science Data Center DAAC doi:10.5067/terra/mopitt/mop03j_l3.007.